Sedimentological analysis of ash-rich pyroclastic density currents, with special emphasis on sin-depositional erosion and clast incorporation: the Brown Tuff eruptions (Vulcano, Italy)

F. Lucchi [a,*], R. Sulpizio [b,c,d], S. Meschiari [a], C.A. Tranne [a], P.G. Albert [e,f], D. Mele [b], P. Dellino [b]

[a] Dipartimento di Scienze Biologiche, Geologiche e Ambientali, Università di Bologna, Piazza Porta S. Donato 1, 40126 Bologna, Italy

[b] Dipartmento di Scienze della Terra e Geoambientali, Universitá di Bari, via Orabona 4, 70125 Bari, Italy

[c] INGV- Bologna section, via D. Creti, 40100, Bologna, Italy

[d] IGAG-CNR, Area della Ricerca di Roma 1- Strada Provinciale 35d, Montelibretti (Rome), Italy

[e] Department of Geography, Swansea University, Singleton Park, Swansea SA2 8PP, UK

[f] Research Laboratory for Archaeology and the History of Art (RLAHA), University of Oxford, Dyson Perrins Building, South Parks Road, Oxford OX1 3QY, UK

[*] Corresponding author

ABSTRACT

The sedimentological, lithological and textural characteristics of the Brown Tuffs (BT) pyroclastic deposits, combined with their grain-size, componentry and geochemical glass compositions, are here investigated to obtain information on the transport and depositional mechanisms of the corresponding pyroclastic density currents (PDCs). The BT are widespread reddish-brown to grey, ash-rich pyroclastic deposits generated by pulsating hydromagmatic explosive activity from the La Fossa Caldera on Vulcano island during the c. 80-6 ka time-stratigraphic interval, and then distributed on most of the Aeolian Islands and Capo Milazzo peninsula (Sicily) and in the Tyrrhenian and Adriatic Sea regions. Near the source area on Vulcano, the BT are characterised by alternating massive and planar to cross stratified lithofacies that result from the stepwise, repeating aggradation of discrete PDC pulses. This alternance is regulated by either fluid escape or granular flow depositional regimes at high clast concentration or grain by grain traction deposition in the waning diluted stages of the PDCs. Most of the BT on Vulcano show intermittently stratified and massive ash deposits resulting from a pervasive post-depositional disruption of the primary structures. This is induced by upward fluid expulsion associated with dissipation of pore pressure between layers at different grain size (fine to coarse ash) and porosity, as outlined by distinctive upwards bends and pillar-type escape structures through the fluid-filled cracks and rupture points. Massive BT deposits with a faint colour and grain-size banding are widely recognised on Lipari, the nearby island of Vulcano. Based on the presence, at the base of BT depositional units, of cm-thick amalgamation bands containing pumice lapilli, scoria and lithic clasts ripped-up and embedded from the loose underlying pyroclastic units, they are interpreted as deposited by ash-rich PDCs laterally spreading from La Fossa Caldera and moving to Lipari. During their motion to Lipari these currents (likely) crossed a narrow and shallow sea-water inlet which did not stop their advancement but influenced the grain size distribution of those spreading on the Lipari mainland. In this paper, the mechanism of clast erosion and incorporation is outlined across the whole island of Lipari by means of field study, grain-size, and geochemical glass analyses on the different components of the mixed basal bands of the BT. This suggests that the BT PDCs maintained enough flow power as to erode the substratum, hence likely impacting the territory, over a distance up to at least 16-17 km from the volcanic source. Evidence that the BT PDCs exerted a high shear-stress over the loose substratum is also provided by undulated, recumbent flame and rip-up structures at the base of some depositional units in southern and central Lipari. In order to form such bed granular instabilities between the BT and the underlying deposits we calculate that the currents had at least a shear velocity of ca. 2 m s^{-1} and a shear stress in the range of 1-4.5 kPa. These results add new insights on the large-scale hazard at the Aeolian Islands and shed new lights on the widespread transport and depositional dynamics of ash flows spreading over the sea and reaching nearby islands, and their interactions with the substratum and the pre-depositional topography.

KEYWORDS

Brown Tuffs, Aeolian Islands, Sedimentary structures, Pyroclastic density current, Clast embedding, Shear-related granular instability structures

1. INTRODUCTION

Pyroclastic density currents (PDCs) are ground hugging mixtures of particles and gas that flow laterally across the topography, and are among the most amazing, complex and dangerous volcanic phenomena (e.g., Carey, 1991; Druitt, 1998; Branney and Kokelaar, 2002; Sulpizio et al., 2014; Lube et al., 2020). Irrespective whether they are concentrated or diluted, PDCs are characterised by a very hostile nature and a complex interplay between transport and depositional mechanisms, which make their study a great challenge for volcanologists. The only way we have to get information about the processes occurring at the time of deposition is to analyse the deposit lithofacies and lithofacies associations in the field (e.g., Sohn and Chough, 1989; Branney and Kokelaar, 2002; Sulpizio et al., 2008a, 2010) or to replicate PDCs in the laboratory (Dellino et al., 2007; 2010; Andrews and Manga, 2012; Sulpizio et al., 2016; Breard and Lube, 2017; Brosch and Lube, 2020). This is particularly demanding for ash rich PDCs that usually have a massive structure and homogeneous lithology, which make a unique sedimentological interpretation challenging. Furthermore, quite rare is in the volcanological literature the analysis of the interaction between PDCs and the pre-depositional topography, which can influence the runout and the internal organisation of the parent currents by means of the bulking due to substratum erosion (Roche et al., 2013; Bernard et al., 2014; Roche, 2015; Pollock et al., 2019).

The Brown Tuffs (BT) deposits, largely outcropping over the Aeolian islands and northern Sicily (Italy), represent an exceptional case-study for shedding light on the elusive processes that drive erosion and deposition in ash-rich PDCs, and their interactions with the substratum. The BT are ash-rich, reddish-brown to grey volcaniclastic deposits from PDCs and associated fallout produced over a long-time span by pulsating hydromagmatic eruptions from the La Fossa Caldera on Vulcano island (Lucchi et al., 2008, 2013b; Cicchino et al., 2011; Meschiari et al., 2020). They usually crop out as massive, moderately to well sorted, fine to coarse ash deposits of meter-scale thickness. Their quite ubiquitous massive appearance, recurring over a wide time span in the stratigraphy of the Aeolian Islands, and the paucity of distinctive sedimentological characteristics have long made it difficult to define the eruptive and depositional mechanisms of the BT. As such, they have been generically interpreted either as primary deposits from PDCs or fallout, reworked deposits from wind-blown volcanic ash (tuff-loess) or even paleo soils (Bergeat, 1899; Keller, 1967, 1980a, 1980b; Pichler, 1980; Crisci et al., 1981, 1983, 1991; Manetti et al., 1988, 1995; Morche, 1988; Losito, 1989; Gioncada et al., 2003). According to the most accepted interpretation, they were emplaced on Vulcano and southern Lipari islands by mostly dilute PDCs, based on the occurrence of rare stratified lithofacies, internal colour and grain-size banding (fine to coarse ash) and topography-controlled thickness variations (De Astis et al, 1997; Lucchi et al., 2008, 2013b; Dellino et al., 2011; De Rosa et al., 2016), although more detailed information on the transport and depositional behaviour of these PDCs has been missing so far. BT deposits cropping out in more distal outcrops on the other islands of the Aeolian archipelago and the Capo Milazzo peninsula were instead related to fallout from a pulsating eruption columns or co-ignimbrite ash clouds (Lucchi et al., 2008).

We present here an in-depth field study of the lithological and sedimentological characteristics of the BT in the proximal and medial-distal outcrops on Vulcano and Lipari islands (Fig. 1A), with the aim of investigating in detail the transport and depositional mechanisms of the corresponding PDCs. Special attention was paid to the evidence of erosion and clast incorporation in the basal portions of some BT depositional units, which were previously signalled by Lucchi et al. (2008; 2013b). Together with the occurrence of shear-related sin-depositional sedimentary structures, this can provide information about the processes occurring in the basal portion of PDCs, which transport the vast majority of the total flow mass (Branney and Kokelaar, 2002; Sulpizio et al., 2014) and determine the threat of these dangerous phenomena (Sulpizio et al., 2014; Dufek et al., 2015; Pollock et al., 2019). In recent times, the erosive capacity of PDCs and their ability to produce sin-depositional substrate deformation by shear forces was studied by means of observations in the field (e.g. LaBerge et al., 2006; Cas et al., 2011; Pollock et al., 2019; Doulliet et al., 2019) or small scale laboratory experiments (e.g. Roche et al., 2013), mostly focused on polydisperse, poorly sorted, concentrated PDC deposits (e.g. those related to the 1980 Mt. St. Helens eruption; Pollock et al., 2019). Nothing has been done, however, on the erosive capability of well sorted, ash rich PDCs. In order to contribute to bridging this gap, we carried out a detail field investigation of the lower portions of the ash-rich BT depositional units supported by grain-size, componentry and geochemical analyses, which helped in deciphering the depositional dynamics of BT PDCs and shed new light on the dispersal dynamics of ash-rich PDCs.

2. GEOLOGICAL SETTING

2.1. Aeolian Islands

The Aeolian Islands (Alicudi, Filicudi, Salina, Lipari, Vulcano, Panarea and Stromboli; Fig. 1B) are the emerged portions of an active volcanic system in the Southern Tyrrhenian Sea, which also includes several seamounts (Barberi et al., 1973; Beccaluva et al., 1985; De Astis et al., 2003; Chiarabba et al., 2008; Ventura, 2013). Aeolian volcanism entirely occurred during the Quaternary, as demonstrated by the oldest radiometric age of c. 1.3 Ma of submarine lavas from the Sisifo seamount (Beccaluva et al., 1985), and then developed subaerially from ~270-250 ka to historical and present times (Leocat, 2011; Lucchi et al., 2013b, and references therein) (Fig. 1C). Successive eruptive epochs of the different volcanic islands have been subdivided by volcanic collapses or major quiescent (erosional) stages (De Astis et al., 2013; Forni et al., 2013; Francalanci et al., 2013; Lucchi et al., 2013a, 2013c, 2013d, 2013e), sometimes associated with episodes of marine ingression and terrace formation during the major sea-level fluctuations (Lucchi, 2009). The marine terraces attributed to the marine (oxygen) isotope stage (MIS) 5, dated between c. 124 and 80 ka (Chappell and Shackleton, 1986; Waelbroeck et al., 2002; Rohling et al., 2014), are well constrained time-stratigraphic markers on most of the archipelago. The erupted magmas in the Aeolian Islands range from basaltic andesites to rhyolites over a large range of differing magmatic suites from calc-alkaline (CA), high-K calc-alkaline (HKCA), shoshonitic (SHO) and K-Series (KS) (Ellam et al., 1988; Francalanci et al., 1993; Peccerillo et al., 2013). Major Violent Strombolian to Sub-Plinian eruptions involving dacite to rhyolite magmas have occurred on Lipari, Vulcano, Salina and Stromboli during the last glacial period (from c. 80 ka) and the early Middle Ages (Crisci et al., 1981; Hornig-Kjarsgaard et al., 1993; Keller and Morche, 1993; Colella and Hiscott, 1997; De Astis et al., 1997a, 2006). This is the time-stratigraphic period when the BT, the object of the present study, were erupted.

2.2. The Brown Tuffs

The BT are widespread, reddish-brown to grey, massive ash-rich volcaniclastic deposits with metric thickness recognised in the Aeolian Islands and the Capo Milazzo peninsula (Sicily).

Chemo-stratigraphic and tephrochronological studies by Lucchi et al. (2008, 2013b) and Meschiari et al. (2020) have documented the BT occurrence, with variable volumes and dispersal areas, on the islands of Vulcano, Lipari, Salina, Filicudi, Stromboli and Alicudi and the Capo Milazzo peninsula, and in Tyrrhenian and Adriatic Sea marine cores, in the c. 80-6 ka time-stratigraphic interval. The BT have been interpreted as the result of PDCs and associated distal fallout related to a pulsating hydromagmatic explosive activity from a source located inside the La Fossa caldera on Vulcano island (De Astis et al, 1997; Lucchi et al., 2008, 2013b; Cicchino et al., 2011) (Fig. 1A). Also, the composition of BT, ranging from K-series (K_2O = 3.3-7.5 wt.%) basaltic trachy-andesites and trachy-andesites through to tephri-phonolites and trachytes (SiO_2 = 49.9-64.1 wt.%; $Na_2O + K_2O$ = 6.5-12.6 wt.%), is entirely consistent with the Vulcano magmatic system (Meschiari et al., 2020).

The BT succession is delimited at the base by marine terraces attributed to the late marine (oxygen) isotope stage (MIS) 5 (c. 124-80 ka) and is subdivided into four macro-units: Lower BT (LBT; 80-56 ka), Intermediate BT (IBT; 56-27 ka), Intermediate-upper BT (IBT-upper; 26-24 ka) and Upper BT (UBT; 24-6 ka). This subdivision is based on the occurrence of interbedded widespread regional or local marker beds, namely the 'Ischia Tephra', equivalent to the Y-7 marine marker tephra (Epomeo Green Tuff, 56 ka; Keller et al., 1978; Tomlinson et al., 2014), the Monte Guardia pyroclastics from Lipari (27-26 ka) and the Spiaggia Lunga scoriae (24 ka) on Vulcano (Fig. 2) (Meschiari et al., 2020). These macro-units are furtherly split into (at least) 16 depositional units, best documented on Vulcano and Lipari islands, where they have variable thicknesses ranging from a few decimetres up to a maximum of 3 m (for each depositional unit), while the entire BT succession has a (cumulated) maximum thickness of 15–25 m on Vulcano and southern Lipari. The different BT depositional units are best distinguished when they are separated by interlayered (local) volcanic units and tephra layers. Between these, the Petrazza Tuffs from Stromboli (77-75 ka) contribute to define the lower chronological constraint of the LBT, whilst the Grey Porri Tuffs (GPT, 70-67 ka) and Lower Pollara Tuffs (LPT, 27 ka) from Salina and the Vallone del Gabellotto tephra from Lipari (8.7–8.4 ka) are important for stratigraphic subdivisions in the LBT, IBT and UBT, respectively (Fig. 2). The Cugni di Molinello scoria bed is an important stratigraphic marker on Vulcano separating the lower and upper portions of the UBT (De Astis et al., 1997; Lucchi et al., 2008, 2013b), which are delimited at the top by the Punte Nere tuffs (5.5 ka). A list of the main features of the units interlayered within the BT succession is provided in the Supplementary File 1. When not intercalated with other deposits, the BT generally appear as lithological homogeneous tephra accumulations that are unlikely to represent single depositional units, but instead they are the amalgamation of different depositional units, as also testified by the occurrence of interlayered localized erosional surfaces and reworked horizons with a limited lateral persistence.

3. METHODS AND TERMINOLOGY

Lithostratigraphic and sedimentological analysis of the BT was carried out on most of the outcrops exposed on the islands of Vulcano and Lipari (Fig. 1A; Table 1), which allow identification (and correlation) of the largest number of depositional units of the BT, relative to all the distinguished BT macro-units (LBT, IBT, IBT-upper and UBT). Following Lucchi (2013), a "depositional unit" is defined as the volcanic (pyroclastic) material deposited during a single, relatively continuous depositional event from PDCs or fallout, and is delimited by evidence of interruptions of deposition (e.g. erosive surfaces, paleo soils, reworked beds, angular discordances) or other sedimentological features (e.g. presence of fine "co-ignimbrite" ash, lithic-rich beds, sharp grain-size variations), and/or by interlayered exotic pyroclastic (including distal tephra layers) or lava deposits.

Outcrop description and sediment logging were based on classical lithostratigraphy and lithofacies analysis, as the main tools to infer the volcanological interpretation of the studied deposits in terms of their transport and emplacement mechanisms (see Branney and Kokelaar, 2002; Sulpizio and Dellino, 2008; Lucchi, 2013 for reviews). Sedimentological investigation of BT units was carried out through lithofacies analysis, which has commonly been used to describe and decipher the deposits of marine and non-marine environments (e.g. Miall, 1978; Lowe, 1982; Mathisen and Vondra, 1983; Miall, 1985; Smith, 1986, 1987; Waresback and Turbeville, 1990; Zanchetta et al., 2004a) and then applied to complex sequences of pyroclastic deposits (Sohn and Chough, 1989; Chough and Sohn, 1990; Colella and Hiscott, 1997; Gurioli et al., 2002; Sulpizio et al., 2007, 2010) and to lateral and vertical variations of sedimentary structures within widespread ignimbrites (e.g. Freundt and Schmincke, 1986; Druitt, 1992; Cole et al., 1993; Allen and Cas, 1998). Lithofacies have been identified in the BT deposits using a combination of texture, sedimentary structures, grain-size and sorting (Table 2). Sedimentary structures were described and measured at cm-scale, and grain-size and component analyses were carried out on selected samples of the mixing bands and reworked bed material at the base of various BT depositional units. Weight % of the size fractions coarser than 3 ϕ (125 μm) at 0.5 ϕ intervals ($\phi = -\log_2 d$), where d is the particle size in mm) were estimated using dry mechanical sieving. The finer fractions, from 3.5 ϕ (63 μm) to 9 ϕ (2 μm), were analysed by means of a Beckman Coulter Multisizer 4 (Mele et al., 2015), and expressed as volume % and successively converted in weight % using a constant clast density assumed equal to that of powdered BT. Component analysis (juvenile, lithics and crystals) was carried out on a representative number of particles of each grain-size fraction of the bulk material. We have differentiated six main classes of components in the size fractions coarser than 3 ϕ (125 μm): i) pumice (white and grey) and ii) scoria of different porphyricity and vesicularity; iii) obsidian fragments; iv) glass fragments; v) crystals; vi) lithic clasts. The finer size fractions are undifferentiated. For the size fractions in the range from 16 to 1.4 mm, a subsample of particles of each component was hand-picked and weighted; the weight fraction of each component was calculated for each size by scaling the number of particles of the subsample to the total weight of the sample. For the grain-size range from 1 to 0.125 mm, particles of each component were counted under a stereomicroscope. The weight of each component was estimated by means of the density of each component in each size fraction. The grain-size statistical parameters by Folk and Ward (1957) were then calculated for the different sub-populations recognised in the samples from the base of BT depositional units by means of the GRADISTAT program (Blott and Pye, 2001; Table 3).

Major and minor element glass data for selected samples of the basal portions of a number of BT depositional units are here provided, referring to the extensive dataset recently made available by Meschiari et al. (2020) for most of the BT depositional units and the interbedded tephra deposits. The samples were mounted in Streurs Epofix epoxy resin and mounts were ground, polished and carbon coated in preparation for chemical analysis. Glass data were determined using a wavelength-dispersive JEOL 8600 electron microprobe (WDS-EMP) hosted at the RLAHA, University of Oxford. Details of the analytical operating conditions, monitoring of data accuracy and precision, and post-analysis data treatment are provided in Meschiari et al. (2020), together with the MPI-DING reference glasses (Jochum et al., 2006). Data presented in plots are normalised (e.g., water-free) and error bars represent reproducibility, calculated as 2X standard deviation of replicate analysis of StHs6/80-G reference glass.

4. RESULTS AND ANALYSES

4.1. Sedimentological features of the BT

Sedimentological analysis of the BT has been carried out on the outcrops exposed on Vulcano and Lipari islands (Fig. 1A), which allow definition of the most complete succession of distinct depositional units of the LBT, IBT, IBT-upper and UBT macro-units (Fig. 2). Most of the outcrops are located in the flattish area of Il Piano on Vulcano island, located southeast of the La Fossa Caldera source area, and mainly belong to the UBT macro-unit. These outcrops are the most proximal today exposed, because the very proximal BT deposits within the inner part of the La Fossa Caldera were affected by the recent collapses in this area or buried below the Holocene deposits of the La Fossa cone (De Astis et al., 2013). Other outcrops of the BT are located to the west of the La Fossa Caldera, near the locality of Grotta dei Pisani, and along the southern flank of Vulcano, near Gelso (Fig. 1A). The BT have been also investigated on a number of outcrops in distinct sectors of the nearby island of Lipari at increasing distances from the source area. The main characteristics of the studied outcrops, and their distance from the source area, are summarized in Table 1.

In most outcrops the BT consist of massive (fine to coarse) ash and show, in places, internal bands of different colours (and grain-size) with gradual contacts (lithofacies mA; Table 2; Fig. 3A). Plane-parallel to cross bedding stratification and lamination (lithofacies psA-xsA; Table 2; Fig. 3B) occur in some exposures on Vulcano and southern Lipari islands, particularly in the UBT deposits (De Astis et al, 1997; Lucchi et al., 2008). Dune bedding with internal cross stratification (having ca. 2-m wavelength and 0.5-m amplitude) are observed in the outcrops of the UBT outside the south-eastern rim of La Fossa Caldera. In the outcrops on Vulcano island, the BT are generally characterised by the alternation of mm to cm thick massive and stratified beds (lithofacies altpsmA), with the occurrence of some laminae of weakly consolidated reddish fine ash. The stratification (and lamination) is generally not laterally persistent and is largely disrupted (lithofacies isA; Table 2; Figs. 3C-F). A typical upward bending of the laminae is observed in many of the fragmentation points (Fig. 3E-H), and in some cases disruption of the laminae occurs in correspondence of mm-scale vertical columns of coarse ash (Fig. 3G-H). The disruption of stratification (lamination) is frequently pervasive, with fragments of laminae distributed unevenly within the massive deposits. It is noteworthy that in a number of outcrops on Vulcano, although seemingly not stratified and unstructured, the BT deposits embed scattered fragments of laminae as relicts of the original stratified/laminated lithofacies (Fig. 3I).

Sin-depositional shear structures (lithofacies mixAL, ucAL, rfAL, ruAL; Table 2) are described and measured at cm-scale at the base of most of the BT depositional units (Figs. 4 and 5), and they are mainly recognised on Lipari rather than on Vulcano (the BT source area). This is probably because of the most common occurrence of interlayered (incoherent) exotic pyroclastic deposits within the BT succession on Lipari, which make the shear structures in the basal portions of the different BT depositional units more evident. In these cases, the basal contacts between BT and exotic deposits are transitional (Fig. 4) and occur as bands of mixed material between the BT and the underlying incoherent pyroclastic deposit (lithofacies mixAL; Table 2). Most of the interbedded pyroclastic deposits are composed of whitish to grey pumice and obsidian of local origin (Punta di Perciato, Falcone, Lip1, Monte Guardia, Vallone del Gabellotto) or grey to dark-grey scoriae and pumice from Salina (Grey Porri Tuffs and Lower Pollara Tuffs), which show a strong lithological contrast with respect to the homogeneous reddish-brown to grey, ash characterizing the BT (Fig. 4). Where two BT depositional units directly overlie each other without a distinguishing layer of exotic pyroclasts, the original thickness and limit between the units cannot be easily recognised (e.g., Fig. 3A), unless it is marked by a minor erosive surface, as occurs in places (Lucchi et al., 2008). This seems the case of the island of Vulcano where the succession of BT is generally made up of distinct, amalgamated depositional units, interlayered only occasionally with exotic pyroclastic deposits. On Vulcano, visible mixing bands occur only when BT units overlie the whitish pumice lapilli and ash of the Monte Guardia and Vallone del Gabellotto fall deposits (Fig. 4G, H) or dark-grey scoriae of the Cugni di Molinello unit. Note that the base of the BT depositional units is sharp when they overly lavas or welded scoriae and other non-erodible pyroclastic deposits, whilst the top contact of BT where they are overlain by other exotic deposits is always sharp (conformable or unconformable).

Over the entire study area (from northern Lipari to southern Vulcano) the lithofacies mixAL occurs independently of the paleo-topography, outcropping even in case of a sub-horizontal paleo topography. Thickness of the mixing bands ranges (approximately) from a few to tens of cm, with a gradual upward transition to the un-mixed BT material (Fig. 4; Table 1) and is arbitrarily measured relative to the level where the original component of BT is dominant with respect to the incorporated clasts from the underlying units. The mixing bands are generally massive, but they show in places alignments of lapilli. The maximum dimension of entrained clasts (either pumice, scoria or lithic) is generally of fine to medium lapilli, although they can occasionally reach sizes of 10 cm (e.g., at the base of BT9 depositional unit in southern Lipari; Fig. 4E). The entrained clasts may be uniformly distributed within a whole BT depositional unit, even if scattered (e.g., Fig. 4F), but in most cases their abundance decreases regularly upwards. When the range of grain sizes of the entrained clasts is broad, reverse grading of the coarse clasts is observed (e.g., Fig. 4E).

Undulated structures consist in basal layers composed of mixed material between the BT and the underlying incoherent pyroclastic deposit that appear as wavy and consisting of alternating crests and troughs (lithofacies ucAL; Table 1). They are recognised in southern and central Lipari at the contact between BT and the underlying pumice units (Fig. 5A-C). Following Pollock et al. (2019), the length of an undulated structure is the distance between successive troughs, and its height is the distance from the lowest part of a trough to the top of the crest. Undulated structures on Lipari have length between 60 and 450 cm and height of ca. 20 cm (Table 1), and they are best exposed in outcrops arranged longitudinally with respect to the BT source area, at distances of 7-10 km (Fig. 5A-C). Crests are almost symmetric and internally massive (Fig. 6B), showing imbrication of coarser clasts in the upper part of the mixed material.

Recumbent flame structures (lithofacies rfAL; Table 2) have an overhanging arm of entrapped clasts from the basal layer that protrudes up into the BT deposit and becomes sub-horizontal and thins in downflow direction (conforming with Pollock et al., 2019). They look very similar to the 'shark fin' structures of Douillet et al. (2019). Recumbent flame structures are common at the base of depositional unit BT9, with the best preserved one documented above the Falcone pyroclastic deposits at Spiaggia Valle Muria, south of Lipari, where the structure has a length of about 60 cm and height of about 20 cm (Fig. 5D). The length is the extent of the deformed zone and the height is the distance from root to top of the sub-horizontal tail. Lithofacies rfAL commonly occurs as trains of pumice and lithic lapilli a few cm above and parallel to the basal contact of the depositional unit BT9 (Fig. 5D). In places, only the trunk of the structure is preserved as an asymmetric deformation of the lapilli from the underlying bed (Fig. 5E).

Rip-up structures (lithofacies ruAL; Table 2), similar to recumbent flame structures, are visible at the base of some depositional units. In these cases, the contact is almost planar, but there are small hook-like structures as asymmetric deformations of the underlying bed, which resemble the trunk of a flame structure (Fig. 5F). These structures are usually few cm in height, and they are bended downcurrent.

4.2. Grain-size and components of the mixing bands of the BT

We collected samples of the mixing bands at the base of some BT depositional units on Lipari island, with the aim of investigating their grain-size distribution and components. The depositional units investigated here cover mostly the stratigraphic interval of the IBT and IBT-upper macro-units, but, as for the grain-size distributions, the results may be considered representative of the entire BT succession because of similar lithology and textural characteristics (Lucchi et al., 2008; De Rosa et al., 2016).

Most samples have a polymodal grain-size distribution (except for sample Lip03/17) and a large number of components (Fig. 6), as widely expected for mixing bands between BT units and the underlying tephra beds. In this respect, each grain-size distribution is the combination of two distinct sup-populations of components, one referred to the BT and the other relative to the underlying pyroclastic deposits. Considering that the Folk and Ward (1957) statistical parameters, like median diameter (Mdϕ) and sorting (σϕ), are not useful for polymodal distributions, we then calculate them in Table 3 for the separated component distributions (and not for the bulk grain-size) recognised in the samples from the base of BT depositional units as in Figure 6.

The BT typically consist of fine (dominant) to coarse ash composed of aphyric, glass fragments (from about 65 to 90 vol. %), from dark brown to brownish and colourless, mostly blocky or poorly vesicular, often slightly altered on their external parts (De Astis et al., 1997; De Rosa et al., 2016). The rest of the BT juvenile components (5–35%) are crystals (clinopyroxene and minor plagioclase, K-feldspar, olivine and amphibole) that are presents as loose fragments or rimmed by glass, with local abundance of mm-size clinopyroxene crystals. Lithic fragments are subordinate in the BT as components of the coarse ash fraction, for a total lithic content usually lower than 5 vol.% (De Astis et al., 1997; Lucchi et al., 2008; De Rosa et al., 2016), except for higher amounts up to 10% in some outcrops of the UBT on Vulcano (De Astis et al., 1997). Diffused dark (to yellowish) scoria lapilli are recognised in different stratigraphic levels of the BT on Vulcano and Lipari (Meschiari et al., 2020).

In carrying out the componentry analyses, we attributed most of the glass fragments and crystals recognised in the fine to coarse ash fractions to the juvenile BT sub-population, along with the (undifferentiated) very fine ash. Loose crystals are considered as components of the BT sub-population, because they lack in the units interlayered to the BT succession. Lithics are kept aside from this analysis because it is not possible to establish which sub-population they belong to. The analysed samples contain variable amounts of exotic components that are correlated to the pyroclastic deposits underlying each of the BT depositional units. These are classified here as 'external components' with respect to the BT sub-population. Specifically, whitish to (minor) grey pumice, and obsidian fragments are recognised in the mixing band at the base of depositional unit BT9 (outcrop L2) and they are fully consistent with the componentry of the underlying Falcone tephra (Gioncada et al., 2005; Forni et al., 2013). Poorly vesicular, highly porphyritic dark scoria and highly vesicular (sub-aphyric) white pumice are reported in the mixing band at the base of deposition unit BT11 in the outcrop L12, as the main components of the underlying bed of the Lower Pollara Tuffs from Salina Island (Morche, 1988; Crisci et al., 1991; Calanchi et al., 1993; Lucchi et al., 2008; Forni et al., 2013). Then, the base of depositional unit BT12 sampled in the outcrops L5, L10 and L12 contain highly vesicular, white (Kf-bearing) pumice, dense to moderately vesicular grey pumice and banded pumice, and variable amounts of obsidian fragments and lithic clasts that are the typical components of the underlying Monte Guardia pyroclastic deposits (De Rosa et al., 2003). A certain amount of sub-aphyric, dark scoria ash fragments are recognised in the depositional units BT9 and BT12 (in outcrops L2, L5 and L10), and they are not present in the underlying Falcone and Monte Guardia units. These scoria fragments are thus included in the componentry of the BT depositional units, in agreement with the report of diffused dark scoria lapilli in different BT outcrops on Vulcano and Lipari (Meschiari et al., 2020). In all the analysed BT depositional units the exotic components are prevalent in the lapilli and block/bombs fractions (Fig. 6), and they have a polymodal grain-size distribution. Glass fragments, crystals and scoria referred to the BT are instead mainly represented in the fine ash fraction. There is not a significant variation of the relative abundance of exotic components with distance from the source area, as evident comparing the grain-size distributions of the BT12 depositional unit in the outcrops L5, L10 and L12 (Fig. 6), at distances from 10 to 14.5 km from the source. However, different quantities of the single grain-size classes and variations of the content of the individual exotic components are reported in these outcrops as a function of the variable lithological features of the underlying Monte

Guardia unit in proximal to distal reaches, relatively to the eruptive vent in southern Lipari. Significant vertical variations of the grain-size parameters are reported for data from different levels of the same BT depositional unit. Specifically, BT12 in the L5 outcrop and BT11 in outcrop L12 were sampled at two stratigraphic levels (Fig. 6), and component analyses show an upward decrease of the content of exotic components, along with an increase in the amount of fine ash.

The analysed sub-populations of the BT, largely devoid of exotic clasts, have all fairly regular and unimodal grain-size distributions, with generally good to moderate sorting (σ_ϕ ranging between 1.29 and 2.07) and Md_ϕ ranging between 3.13 and 4.97 (Fig. 6). These values are roughly consistent with the pattern obtained by De Astis et al. (1997) for the UBT on Vulcano which defines a trend of regularly decreasing median and better sorting from proximal (σ_ϕ=0.8-1.8 and Md_ϕ=1.7-2.5 at distances of 1.5-2.0 km) to more distal locations (σ_ϕ=1.0-1.2 and Md_ϕ=3.0-3.5 at distances of 4.0-4.5 km) from the source. However, not all BT samples on Lipari fit this trend perfectly, as shown for example by the median value of 1.98 for the LIP02/17 sample in central Lipari and the moderate sorting of some samples in different sectors of Lipari. On this, we argue that the data for the BT sub-populations may be not totally depurated from the presence of external components related to the embedded lapilli and ash from the underlying units.

We also calculated the Sauter mean diameter (Sauter 1926) of the different grain size distributions (Table 3). The Sauter mean diameter is a length-scale parameter useful in characterizing fluidization processes in granular materials (Kowalczuk et al., 2016), because it defines the area-weighted mean particle size, which is important to estimate the drag applied onto particle surfaces. Because our BT sub-populations are mostly unimodal and Gaussian like, we used the method of Breard et al. (2019):

$$D_{32}(mm) = 2^{-[\mu_\varphi + \frac{ln2}{2}\sigma_\varphi^2]} \quad (1)$$

where μ_ϕ is the mean of the grain size distribution and σ_ϕ is the sorting. The values of the Sauter mean diameter of BT sub-populations range from 0.22 mm to 0.03 mm (Table 3), which results in a minimum permeability in the order of 10^{-10} – 10^{-12} m^2 (Breard et al., 2019).

4.3. Geochemical components of the mixing bands of the BT

A number of the BT depositional units investigated on both Lipari and Vulcano islands contain minor populations of exotic volcanic glass compositions that mostly plot well outside the dominant K-series compositional field of the BT, which ranges from basaltic trachy-andesites and trachy-andesites through to tephri-phonolites and trachytes. The exotic glass compositions are here named 'secondary components' consistent with Meschiari et al. (2020) (Fig. 7A, B). These secondary components are generally reported from the basal portions of the individual BT depositional units, characterised by mixing bands with the underlying pyroclastic deposits (lithofacies mA), and chemically similar to these deposits. Figure 7 provides clear evidence of the geochemical correspondence between the secondary components identified within depositional units belonging to the LBT, IBT, IBT-upper and UBT macro-units and the underlying pyroclastic units sourced from eruptions on Salina (Grey Porri Tuffs), Lipari (Punta del Perciato, Falcone, Lip1, Monte Guardia, Vallone del Gabellotto) and Vulcano (Cugni di Molinello), following the reconstructed stratigraphic succession (Fig. 2). Major and minor element glass analyses of representative samples relative to different BT depositional units and their secondary components are reported in the Supplementary File 2.

Among the analysed samples there is only one apparent lack of geochemical agreement between a BT secondary component and the underlying deposits. Specifically, the BT8 depositional unit (sample bt12/16), belonging to the IBT, directly rests above the Punta del Perciato pumice and ash in the L2 outcrop of Lipari. While it contains secondary rhyolitic glasses that are compositionally similar at a major element level to the Punta del Perciato glasses, some of these secondary glasses exhibit significantly higher K_2O and lower Na_2O contents relative to the Punta del Perciato glasses (Figs. 7C, D, E). These offsets could reflect compositional variability in the underlying Punta del Perciato tephra unit which may have been previously undetected, considering that its previous chemical characterisation targeted only the pumice component (Albert et al., 2017). An alternative explanation is that hydration has resulted in alkali exchange within these particular glass fragments. This is apparently supported by previous IBT investigations by De Rosa et al. (2016) who identified physical evidence of fluid induced alteration (hydration) of the juvenile glass particles relating to the sin-eruptive interaction of magma and hot fluids or seawater. Indeed, our attempt to chemically analyse juvenile glass components of BT8 was entirely precluded by the significant alteration of the dominant glass component.

It is noteworthy that in some cases secondary components are also reported in BT depositional units where mixing with underlying pyroclastic deposits is not visible at a macroscopic scale. In south Lipari (outcrop L2) we sampled the IBT (sample bt14/16) that rests above the Falcone pumice succession, which are commonly subdivided into the depositional units BT9 and BT10 by the interlayered Lip1 tephra unit (Fig. 2). The sample bt14/16 contains HKCA rhyolitic secondary glass components that are broadly consistent with the Lip 1 ash (Figs. 7C, D, E), although this tephra layer is not visible in the investigated outcrop. A possible correlation of the HKCA rhyolitic secondary glass components found in bt14/16 with the underlying Falcone pumice unit is considered not probable because this sample was taken close to the base of the (overlying) Lower Pollara Tuffs, at about 2 meters above the contact with the Falcone unit. A similar situation is noticed at the Punta della Crapazza outcrop (L0) in the IBT sampled above the Falcone domes (samples LIP15/18, LIP16/18). In these samples we do observe HKCA rhyolitic secondary glasses which are chemically consistent with the Lip1 tephra layer (Figs. 7C, D, E), although the latter is not visible in the investigated stratigraphic succession. A correlation of these secondary components with the Falcone unit, which could be chemically possible, is considered unreasonable because the sampled IBT rests above the thick lava domes erupted after the Falcone pumice succession. Finally, at the outcrop of Monterosa (L7) we sampled the IBT (sample LIP45/17) above the Ischia Tephra, and none of the interbedded stratigraphic markers from southern Lipari are visible (e.g., the Punta di Perciato, Falcone and Lip1). However, in sample LIP45/17 we do find chemical evidence of secondary HKCA rhyolitic glass components that could be attributed to any of the above-mentioned tephra units (Figs. 7C, D, E).

5. DISCUSSION

In the following, we will discuss the evidence of an origin of the BT deposits on the islands of Vulcano and Lipari from PDCs, and their specific transport and depositional mechanisms. We will not include in this discussion the BT deposits cropping out on other islands of the Aeolian archipelago or in the Sicily mainland, which do not have the same characteristics of lithofacies indicative of a PDC deposition. On this, we rely on the previous interpretation that the BT recognized further distally from the La Fossa Caldera source in the other islands of the Aeolian archipelago and Capo Milazzo in Sicily reflect fallout processes from a pulsating eruption column or co-ignimbrite ash clouds (Lucchi et al., 2008), whilst distal ash layers are recorded in Tyrrhenian and Adriatic Sea marine cores (Meschiari et al., 2020). This reflects the high mobility of fine ash in the atmosphere, which can be dispersed by both high and low atmosphere dynamics due to their long settling times (Sulpizio et al., 2008b; 2013; Giaccio et al., 2008).

5.1. Model for deposition from the BT PDCs

PDC deposits record processes occurring in the flow boundary zone, which includes the lowermost part of the current interacting with the forming deposits or with the topography (Branney and Kokelaar, 2002). Most PDC deposits originated from stratified flows in which the segregation of the particles with higher terminal velocities in the lowermost part can result in the development of a high concentration zone (Valentine, 1987; Branney and Kokelaar, 2002; Dellino et al., 2004; Sulpizio et al., 2014). This basal portion of the flow can move downslope developing different depositional regimes, which can span from traction- to granular flow-dominated (see Branney and Kokelaar, 2002; Sulpizio et al., 2014; Lube et al., 2021; for a review of internal structures and processes). In polydisperse mixtures, including a wide range of sizes (from ash to blocks) and componentry (lithics, pumice, crystals), sedimentary structures may help in deciphering the depositional regime at time of deposition, defining the lithofacies of the deposit. As an example, sedimentary structures like parallel to cross stratification and dune-bedding are indicative of traction-dominated depositional regime from a flow-boundary zone of a diluted PDC (e.g., Andrews and Manga, 2012; Doulliet et al., 2019). At the other end of PDC spectrum, reverse grading of coarse clasts may indicate a granular flow-dominated depositional regime in a concentrated PDC, in which grain interaction can induce kinetic sieving and kinematic squeezing of the largest particles (e.g., Felix and Thomas, 2004). If the porosity within the flow-boundary zone is sufficiently low to maintain the gas entrapped in the mixture, a fluid escape-dominated depositional regime may develop, with deposits that appears massive and poorly sorted. Well selected, ash dominated deposits are generally interpreted as gentle settling of fine-grained particles from a diluted cloud, defining a direct fallout regime.

These sedimentological hints are of little significance to interpret the features of PDCs formed only by well selected ash particles, as in the case of most of the BT deposits (Figs. 3-5). This is because of the impossibility to develop sedimentary structures from very fine grain-sizes (Dellino et al., 2019), which makes difficult to interpret the depositional regimes of ash-rich PDCs from lithofacies analysis. This is one of the reasons why it is complicated to decipher the transport and depositional mechanisms of the PDCs of the BT eruptions, which were previously generically interpreted as mostly dilute PDCs or fallout from co-ignimbrite ash clouds or accompanying eruption columns (De Astis et al., 1997; Lucchi et al., 2008).

Most of the information on the depositional mechanisms of the BT presented here is derived from distinctive lithofacies mA, psA and xsA (Table 2) recognised in the proximal outcrops of the UBT macro-unit on Vulcano island (outcrops V1-V4; Fig. 1A). Massive deposits of the lithofacies mA are interpreted as the result of the deposition from slow-moving, ground-hugging ash-rich PDCs, and their homogeneous appearance is indicative of fluid escape or granular flow depositional regimes from a fine-grained, concentrated flow-boundary zone. The abundant ash aggregates present in these deposits at the microscopic scale (Lucchi et al., 2008) indicate the occurrence of steam in the ash cloud or fine ash aggregation driven by electrostatic force during the gentle settling of ash from the more diluted portions (or the phoenix cloud) of the PDCs. Lithofacies psA and xsA instead indicate grain by grain deposition from dilute and turbulent PDCs, mainly formed by coarse and fine ash, in which suspension and traction are the main transport (and depositional) mechanisms. Notably, in the UBT deposits investigated here, the most common is lithofacies altpsmA (Fig. 3; Table 2). This is a combination of lithofacies mA and lithofacies psA, and is indicative of a stepwise, repetitive aggradation of discrete PDC pulses developed within each depositional unit of the BT. Massive beds are deposited from granular- or fluid-escape dominated depositional regimes of concentrated PDCs and alternate with stratified ash from the turbulent and diluted ash cloud accompanying the underflow during the waning stage of each pulse. This depositional behaviour is consistent with the long-lasting, pulsating eruptive activity that is assumed to have characterised the emplacement of the UBT macro-unit (and the rest of the BT) on Vulcano island (Lucchi et al., 2008, 2013b).

However, intermittently stratified ash deposits of the lithofacies isA (Fig. 3) are the most prominent on Vulcano island and characterise most of the BT outcrops on Il Piano area. This lithofacies is not interpreted as a primary feature acquired at time of deposition of the PDCs during the BT eruptions, but as the result of pervasive post-depositional disruption of the primary deposits of lithofacies altpsmA. The disruption of stratified beds here is explained as due to fluid escape related to dissipation of pore pressure from the underlying massive beds occurred during or immediately after the emplacement of the individual beds (Fig. 8). This mechanism of fluid expulsion resembles that largely described in marine and fluvial sedimentary environments (Allen, 1977; Owen, 1987; Selker, 1993; Owen, 1996; Odonne et al., 2011), and even in pyroclastic deposits (Douillet et al., 2015). Experiments have demonstrated that fluid expulsion structures can be produced by an unstable fluidization behaviour where a lower base layer of granular material is inhibited from releasing intergranular fluids by the presence of an overlying low porosity top layer (Nichols et al., 1994). The weight of the overlying material is balanced by an increased fluid pressure in the basal layer. If the load exceeds a critical threshold, a fluid-filled crack forms and, as it grows, instability causes the top layer to bend (Fig. 3G). Rupture occurs at the apex of fluid crack, allowing the underlying fluid and fluidized material to burst out through the top layer. The fluidized base layer material then flows through the rupture until the fluid overpressure is fully dissipated. The top layer material is bent upwards around the rupture (Figs. 3E, G, H), and the resulting pillar-type escape structure is preserved (Figs. 3G, H). The vigour of the burst out is greatest when the base layer material has a grain-size 15% of the top layer material (Nichols et al., 1994), as in the case of the BT investigated here that are composed of coarse to fine ash deposits. If the base layer grain-size is less than 8% of the top layer then base layer material will pass through the top layer pore spaces, without forming an escape structure. Depending on how much the disruption mechanism was pervasive, the BT deposits in the investigated outcrops have either largely preserved the original lithofacies (Fig. 3F) or they are almost entirely massive with only fragments of laminae distributed unevenly as relicts of the original stratified lithofacies (Fig. 3I). It is therefore important to note that in many cases the massive deposits of the BT on Vulcano are not a primary lithofacies, but they are instead the result of pervasive post-depositional fluid escape processes occurred during or immediately after their emplacement. De Astis et al. (1997) suggested that the fragments of stratified ash embedded in some massive BT deposits was due to fragmentation of a stratified layer due to an external trigger (earthquakes), with subsequent sinking of the denser and heavier fragments into the soft massive deposits. We consider this explanation less probable because the evidence of disrupted stratification and fragments of stratified ash is recognised in a number of BT depositional units at different stratigraphic levels, which makes it difficult to assume a repetitive trigger external to the depositional system. Moreover, the upward bending of the fragmentation points and pillar-type structures observed in the lithofacies isA are more consistent with a model of fluid escape. Small ash diapirs were explained by De Astis et al. (1997) as a result of a significant amount of (liquid) water in the massive deposits, but we consider more probable a process of fluid escape due to dissipation of the pore pressure during deposition of the BT and subsequent compaction.

Most of the BT outcrops on Lipari and southern Vulcano are characterised by homogeneously massive lithofacies that are referred to deposition from PDCs on the base of significant thickness variations as function of paleo-topography of the individual BT depositional units, which is not fully consistent with primary fallout processes (Lucchi et al., 2008). Progressive aggradation of different PDC pulses can be argued from faint banding due to colour differences or subtle grain-size variations within massive deposits. Also, in this case the deposits are mostly formed by ash, which raises the issue if they were erupted as mixtures of fine particles or if the coarse particles were deposited in very proximal areas. It was suggested that an efficient hydromagmatic fragmentation have produced a large amount of fine ash with respect to lapilli and blocks. Evidence that fragmentation was driven mostly by magma-water interaction is provided by SEM results showing that equant blocky fragments, with quenching cracks and abundant adhering particles are dominant in the BT deposits (De Astis et al., 1997; Lucchi et al., 2008). This is consistent with a location of eruptive vents inside the La Fossa Caldera, the floor of which might have been below or near sea level during most of its evolution starting from c. 80 ka (De Astis et al., 2013). Another possible explanation, which may be concomitant with efficient hydromagmatic fragmentation, is that coarse-grained material has been probably deposited in the caldera depression, which is now filled and completely covered with the more recent deposits of La Fossa cone (De Astis et al., 1997; Lucchi et al., 2008). For the deposits outcropping on Vulcano island, it must be considered that decoupling of basal (coarse-grained) and upper (fine-grained) parts of the PDCs has occurred when the PDCs impacted against the caldera walls (Fig. 8), with only the finer grained parts transported by turbulence in the ash clouds able to overpass the topographic obstacle and spread over the central and southern parts of Vulcano island.

The massive BT deposits can be interpreted either as the result of direct fallout-dominated flow-boundary zones or fluid-escape (or even granular flow) depositional regimes in well sorted, ash-dominated pyroclastic mixtures (cf. Branney and Kokelaar, 2002; Sulpizio et al., 2007; 2010). Direct fallout implies mainly vertical gentle settling of particles in a slow moving or motionless pyroclastic cloud, whilst deposition from granular flow or fluid-escape dominated flow-boundary zones implies lateral movement of the moving flow. The key feature for establishing a depositional mechanism from laterally spreading PDCs is the evidence at the base of the BT depositional units of mixing bands containing a substantial component of ash and lapilli made up of pumice, scoria and lithics from the underlying pyroclastic deposits (lithofacies mixAL; Fig. 4). These mixing bands indicate erosion and incorporation of loose material from the underlying beds into the moving ash flows that deposited the BT. The general poor sorting and massive appearance of the mixed deposits are suggestive of sedimentation from a current in which the rate of supply (Rs) is higher than the rate of deposition (Rd), which induces rapid development of a highly concentrated zone above the flow boundary, dominated by a granular flow (or fluid-escape) depositional regime. The moving flows relative to the BT exerted shear stress over the loose, erodible pyroclastic deposits that represented their substratum, causing entrapment of exotic clasts into the flow body (Fig. 9). The reverse grading of entrained coarse clasts observed in some places (e.g. Fig. 4E) suggests that a lateral movement under high shear occurred during transportation and deposition of the BT PDCs. Such reverse grading of coarse clasts is attributed to dispersive pressure processes induced by grain-grain collision in a high-concentration zone at the base of the current (Lowe,1982; Sohn,1997; Dellino et al., 2004).

Clast embedding at the base of BT deposits was previously signalled by Lucchi et al. (2008) only in the outcrops of southern Lipari and Gelso (south Vulcano; Fig. 1A), whilst here we document the occurrence of entrainment processes across the entire study area, from northern Lipari to central and southern Vulcano, thus substantially enlarging the area where there is evidence of substrate erosion exerted by the BT PDCs. The mixing bands are easily recognised in the field where the eroded/remobilized bed is made of lapilli (due to the contrasting grain-size) or light-coloured clasts (due to contrasting colour), as also supported by grain size and component analyses of selected base layers of BT depositional units (Fig. 6). When the mixing material is not visible at visual inspection, it can be documented by secondary glass components plotting outside of the main compositional field of the BT (Fig. 7). As an example, the rhyolitic Lip1 (ash) tephra layer from an eruptive vent in southern Lipari is characterised by a very discontinuous areal distribution. This can be due to processes of wind-reworking or post-depositional erosion, as typically occurs for ash beds, but the role played by processes of erosion and clast incorporation by the BT currents is clearly outlined by the finding of secondary components chemically correlated to Lip1 within the BT depositional unit above (Fig. 7C-E), even where there is no direct evidence of the Lip1 tephra layer in the field.

Overall, sedimentological analyses, combined with grain-size, componentry and geochemical investigation, provide unequivocal evidence that the BT were deposited from PDCs laterally spreading from the La Fossa caldera all over the islands of Lipari and Vulcano. De Rosa et al. (2016) suggested that mixing bands are the result of post-eruptive remobilization of the BT deposits on pre-existing steep slopes. The occurrence of mixing bands even on flat topography make us confident in excluding reworking as a primary mechanism. Notably, the evidence of mixing bands at the base of distinct BT depositional units even in the northern sector of the island of Lipari enlarges the area where the PDCs that deposited the BT had a potential of eroding the substratum and embedding clasts from the underlying units up to distances of 16-17 km from the source area, therefore substantially increasing the estimate of the maximum run-out of currents of this type. This is coherent with experimental models (Girolami et al. 2008; Roche et al. 2008; Cagnoli and Romano 2010; Dellino et al. 2019) showing that PDCs transporting mostly fine ash, like those of the BT on Lipari, may travel further and possess a higher capacity of impact over the territory with respect to those characterised by coarser material. On this, the calculated values of Sauter median diameters (Table 3) indicate very low porosity of the BT pyroclastic mixture in the flow boundary zone (in the order of 10^{-10}–10^{-12} m^2), which suggests long time retention of gas within the mixture enhancing fluidization and flow mobility (Druitt et al. 2007; Smith et al., 2018; Lube et al. 2019; Roche et al., 2021).

It cannot be excluded that a significant part of proximal to medial massive BT deposits on Vulcano and Lipari, where evidences of shear structures or exotic component mixing are absent, is the result of ash fallout from co-ignimbrite ash clouds or eruption columns, a process that is suggested to be dominant in the more distal outcrops in the other islands of the Aeolian archipelago and the Capo Milazzo peninsula. Given the cryptic nature of the BT deposits where the contacts between different depositional units cannot be easily recognised, the volume fraction of the ash deposits possibly deposited from fallout processes could not be discerned. This does not weaken the evidence from sedimentological characteristics, which indicates a dominant deposition of the BT on Lipari and Vulcano from ground hugging PDCs.

The fine-grained, well sorted grain size of BT deposits is unusual for PDCs deposits recognised widely and apparently crossing between adjacent islands and deserves some further consideration and discussion. It is notable that the islands of Vulcano and Lipari are currently separated by the narrow and shallow sea-water inlet of Bocche di Vulcano with a minimum depth of c. 40 m and width of less than 1 km. Considering that most of the 80-6 ka time-stratigraphic interval of the BT has elapsed in lowstand conditions (Rohling et al., 2014), this sea-water inlet might also have been for a long time narrower and shallower. This means that most of the PDCs that deposited the BT on Lipari mainland had to overcome a small sea inlet which did not actually hinder their lateral spreading but might have influenced their transport and depositional behaviour. The PDCs that passed over the sea inlet in fact had to have density lower than sea water (i.e., less than 1025 kg/m^3). This is an unrealistic density for the basal part of any PDCs, in which the density stratification induces packing of solid particles with density usually in excess of that of water. Therefore, it can be reasonably assumed that the basal, coarser and more concentrated portion of PDCs spreading from Vulcano sunk into the sea water accompanied by decoupling of the turbulent, more diluted portion of the PDCs which was able to pass over the sea and reach the Lipari mainland (Fig. 10). This water density bias and the decoupling of the basal and upper portions of the PDCs could explain the grain size characteristics of the BT deposits on Lipari island. When these PDCs reached Lipari they encountered a rugged and irregular topography due to the presence of a rhyolitic dome complex emplaced between c. 50 and 20 ka. The flow of diluted and turbulent PDCs over variable slopes produced loss of momentum, which reflected in loss of turbulence and less capacity to maintain solid particles in suspension. This produced an increased concentration of particles in the flow boundary and transition to dominant granular flow or fluid-escape regimes at time of deposition (Fig. 10). Lithofacies analysis indicates that the BT PDCs mostly deposited in granular flow or fluid escape regimes due to interaction with the paleo-topography and increased sedimentation rate, whilst the currents travelled large distances in a dilute and turbulent behaviour reaching distances around 16-17 km from the source (up to northern Lipari). The (more) concentrated basal portions of these PDCs were generally able to erode the incoherent substratum embedding clasts from the underlying units and produced sin-depositional shear structures (see below). In any case, the distance travelled by PDCs (around 16-17 km) suggests high mass discharge rates feeding the currents spreading from the vent (Roche et al., 2021).

5.2 Physical characteristics of the PDCs inferred from shear structures

In addition to the mixed lithofacies, also the sedimentary structures of lithofacies ucAL, rfAL, ruAL recognised in outcrops of southern and central Lipari are indicative of an effective lateral transport and shear stress exerted by the ash flows of the BT over the substratum (Fig. 9).

In particular, the undulated contacts (lithofacies ucAL) between the BT depositional units and the underlying lapilli beds in outcrops L1 and L5 may be referred to conditions of high shear stress exerted by the overriding currents to the loose lapilli substratum, which induces remobilization of its upper part and formation of waves with variable wavelength and imbrication of coarser clasts. Such imbrication testifies for the occurrence of traction carpet processes, in which the static bed material is moved and reorganised in a frictional regime by the overriding flow (e.g. Sohn, 1997; Dellino et al., 2004). Recumbent flame structures (lithofacies rfAL) also indicate high shear stress exerted by the overriding PDCs of the BT eruptions over the underlying lapilli beds, which produce incorporation of lapilli that are aligned downflow and bended to form an alignment of lapilli within the BT ash deposit for a distance up to some meters. Instead, the small hook-like structures of the lithofacies ruAL is related to conditions of moderate shear stress exerted from the overriding ash flow, which was able to rip-up lapilli from the underlying bed into the BT unit but with no significant lateral displacement of the upper part of the structure. The formation of the different shear structures depends on both flow and erodible deposit characteristics, like flow velocity, depositional regime, perpendicular load component of the moving flow, grain packing in the deposit, and terminal velocity of erodible clasts, among others. Currently, there are few laboratory experiments on entrapment of loose substratum into the moving flow, carried out using synthetic material (Roche et al. 2013, 2016; Roche 2015). They mainly focus on clast entrapment due to underpressure at the head of the moving flow, a process different from that here described, which does not produce the observed syn-depositional shear structures. In order to unravel the flow conditions responsible of the various deposit characteristics and structures some hints may be gained from published studies on PDC erosion based on field evidence. Following Doulliet et al. (2019) and Pollock et al. (2019), the recumbent flame structures are referred to PDCs of similar concentration to the undulated structures, and the latter represent an earlier phase of growth of the recumbent flame structures. Moreover, the recumbent flame structures are a reliable indicator of the approximate local direction of the currents. Additionally, the recumbent flame structures are related to conditions of high concentration in the flow boundary zone (Pollock et al., 2019), indicating that the BT were deposited by mostly concentrated PDCs.

By a physical point of view, the undulated (lithofacies ucAL), recumbent flame (lithofacies rfAL) and rip-up structures (lithofacies ruAL) recognised at the base of BT depositional units are a signature of instabilities occurring at the boundary of two sheared granular media, and they may represent the frozen record of granular, pseudo-Kelvin–Helmholtz instabilities. Waves and overturned stratification like those described at the base of BT are usually the result of simple shear exerted by the overriding flow on the loose substratum (Allen and Banks, 1972; Mills, 1983; Valentine et al., 1989; Røe and Hermansen, 2006; Douillet et al., 2015; Pollock et al., 2019). They have been also described in several analogue experimental studies with granular flows over grain beds (Goldfarb et al., 2002; Mangeney et al., 2010; Rowley et al., 2011; Roche et al., 2013; Farin et al., 2014).

Shear stress τ is defined as:

$$\tau = u_*^2 \rho_{PDC} \quad (2)$$

where u∗ is the shear velocity, and ρ_{PDC} is the current density. The minimum velocity needed for starting bed instability is given by:

$$u_{*min} = \left[\frac{g\lambda}{2\pi}\frac{(1-x^2)}{x}\right]^{1/2} \quad (3)$$

where *g* is the gravity acceleration, λ is the wavelength of bed instability, and *x* the relative flow concentration (ρ_{PDC} / ρ_{bed}) (Doulliet et al., 2015). Eq. (3) states that the wavelength of the instabilities depends on shear velocity and the ratio between particle concentrations of the PDC and the underlying bed. It is interesting to note that Eq. (3) holds for $0 \leq x \leq 1$ (Douillet et al., 2015), which means that instabilities can form only if particle concentration in the bed is greater than that in the flow. Figure 11 shows that the more diluted the flow is (lower numbers of *x*), the more is the velocity required to form bed instabilities. In all PDCs the solid-void ratio and flow density (ρ_{PDC}) can vary greatly with height, producing flow stratification (e.g., Valentine, 1987; Dellino et al., 2004), and developing granular flow or fluid-escape dominated flow-boundary zones. The fluid and solid components abundance and densities determine the physical properties of the flow, which greatly depend on grain-size distributions and relative abundance of the different solid componentry. Without direct measurements, a gross estimate of particle concentration and ρ_{PDC} can be obtained from the deposits for granular/fluid escape-dominated flows. Assuming a characteristic solid-fluid ratio of 50-60% for ash rich deposits and a mean solid density of 2400 kg m^{-3} (e.g., Sulpizio et al., 2007; Breard and Lube, 2017; Lube et al. 2019), it results a range of ρ_{PDC} of ca. 1100-1400 kg/m^{-3}. Considering that the solid volume fraction can reach 70% in PDC deposits (Gase et al., 2018) and assuming a flow concentration of 50-60 vol.%, it results in a relative flow concentration *(x)* of 10-20% lower than the deposit, which can be used to constrain the minimum shear velocity to form the observed bed instabilities. For wavelength number of 0.16 (l=40 cm) the minimum basal shear velocity is less than 1 m s^{-1}, while for wavelength number of 0.72 (l=450 cm) it is less than 2 m s^{-1} (Fig. 11), a value comparable to that obtained for the Peach Spring ignimbrite (Roche et al., 2016). It is to note that the calculated velocities do not reflect velocities at the flow front, but instead reflect the basal slip velocity at the time of instability formation. The resulting minimum basal shear stress, which refers the very base of the stratified current (a few mm-cm) may be calculated in the range of 1-4.5 kPa using Eq. (1).

6. CONCLUSIONS

A sedimentological analysis of lithofacies, combined with grain-size and componentry investigation and grain-specific volcanic glass compositional data, for a large number of the different depositional units of the ash-rich Brown Tuffs (BT) has been carried out on Lipari and Vulcano to provide constraints on their transport and depositional mechanisms and dispersal area. We rely on the framework of knowledge acquired so far according to which the BT were generated over a long-time interval between c. 80 and 6 ka by pulsating hydromagmatic eruptions from eruptive vent(s) inside the La Fossa caldera on Vulcano. The following are the main outcomes of the present work:

1. The UBT on Vulcano (24-6 ka) are deposited from ground-hugging ash-rich pyroclastic density currents (PDCs) that have surmounted the caldera walls. Alternating massive and planar to cross stratified deposits reflect a repetitive aggradation of PDC pulses characterised by either fluid escape or granular flow depositional regimes from a fine-

grained, concentrated flow-boundary zone (lithofacies mA) or grain by grain deposition from dilute and turbulent PDCs (lithofacies psA-xsA) during the waning stage of each pulse.

2. Intermittently stratified ash deposits of the UBT on Vulcano, with distinctive upwards bends and pillar- type escape structures through the rupture points are interpreted as the result of post-depositional disruption of the primary deposits due to fluid escape related to dissipation of pore pressure between layers at different porosity. This process can be pervasive to produce almost entirely massive UBT deposits with only fragments of laminae distributed unevenly as relicts of the original stratified lithofacies.
3. Most of the BT on Lipari are emplaced by PDCs that have likely travelled over a narrow sea inlet. The water density bias produced decoupling of basal denser parts of the currents, which sunk into the sea, from the turbulent and more diluted upper parts, able to reach Lipari. This induced selection of particles and accounts for the unusual good sorting and very fine grain size distribution of BT deposits on Lipari island. Topography-induced decoupling occurred on Vulcano due to the interaction of southwards laterally spreading PDCs with the La Fossa Caldera walls. Most of the BT on Lipari and partly on Vulcano were deposited in fluid escape or granular flow regimes induced by the interaction of the turbulent parent flows with the paleo-topography, which caused loss of turbulence and concentration of the solid particles in the flow boundary zone.
4. Most of the individual BT depositional units on Lipari (and Vulcano) are characterised at the base by mixing bands containing pumice, scoria and lithic clasts ripped-up and embedded from the loose underlying pyroclastic units, as outlined by field study supported by grain-size and component analyses and geochemical glass investigation of the different components. These mixing bands indicate erosion and incorporation of loose material from the underlying beds into the laterally spreading ash flows that deposited the BT. The recognition of these structures up to the northern sector of Lipari indicates that the PDCs

during the BT eruptions travelled up to distances of (at least) 16-17 km from the source area and possessed a high capacity of impact over the territory.

5. Undulated, recumbent flame and rip-up structures are recognised at the base of some BT depositional units on southern and central Lipari as the result of effective lateral transport and moderate to high shear stress exerted by the ash flows of the BT to the substratum. These structures provide indications on the approximate local south-to-north direction of the currents, and the conditions of high solid concentration of the PDCs that deposited these BT. Moreover, they can be adopted to estimate a basal shear velocity of the currents of up to c. 2 m s^{-1} and a shear stress in the range of 1-4.5 kPa at the time of structure formation.

In conclusion, massive ash deposits of the BT can actually result from the spreading of PDCs that possess a high erosive power and shear strength at the flow base, representing a substantial hazard for tens of km away from the source area, which is amplified by the fine grain size that helps maintaining fluidization and increasing flow mobility.

ACKNOWLEDGEMENTS

We thank three anonymous reviewers for their thoughtful suggestions to the first draft of this manuscript, and Catherine Chagué for her kind and careful editing. Sara Meschiari was funded through a Ph.D. Scholarship of the University of Bologna-Alma Mater Studiorum. Paul G. Albert was funded through a UKRI Future Leaders Fellowship (MR/S035478/1).

REFERENCES

Albert, P.G., Tomlinson, E.L., Smith, V.C., Di Traglia, F., Pistolesi, M., Morris, A., Donato, P., De Rosa, R., Sulpizio, R., Keller, J., Rosi, M., Menzies M., 2017. Glass geochemistry of pyroclastic deposits from the Aeolian Islands in the last 50 ka: a proximal database for tephrochronology. Journal of Volcanology and Geothermal Research 336, 81-107.

Allen, J.R.L., 1977. The possible mechanics of convolute lamination in graded sand beds. Journal of the Geological Society London 134, 19–31.

Allen, J.R.L., Banks, N.L., 1972. An interpretation and analysis of recumbent folded deformed cross bedding. Sedimentology 19, 257-283.

Allen, S.R., Cas, R.A.F., 1998. Rhyolitic fallout and pyroclastic density current deposits from a phreatoplinian eruption in the eastern Aegean Sea, Greece. Journal of Volcanology and Geothermal Research 86, 219–251.

Andrews, B.J., Manga, M., 2012. Experimental study of turbulence, sedimentation, and coignimbrite mass partitioning in dilute pyroclastic density currents. Journal of Volcanology and Geothermal Research 225-226, 30-44.

Barberi, F., Gasparini, P., Innocenti, F., Ferrara, G., Villari, L., 1973. Volcanism of the southern Tyrrhenian Sea and its geodynamic implications. Journal of Geophysical Research 78, 5221-5232.

Beccaluva, L., Gabbianelli, G., Lucchini, F., Rossi, P.L., Savelli, C., 1985. Petrology and K/Ar ages of volcanics dredged from the Aeolian seamounts: implications for geodynamic evolution of the Southern Tyrrhenian basin. Earth and Planetary Science Letters 74, 187–208.

Bergeat, A., 1899. Die Äolischen Inseln (Stromboli, Panaria, Salina, Lipari, Vulcano, Filicudi und Alicudi). Abhandlungen der Mathematisch-Physikalischen Klasse der Königlich Bayerischen Akademie der Wissenschaften, vol. 20 I. Abt., München, 274 pp (in German)

Bernard, J., Kelfoun, K., Le Pennec, J.-L., Vallejo Vargas, S., 2014. Pyroclastic flow erosion and bulking processes; comparing field-based vs. modeling results at Tungurahua Volcano, Ecuador. Bulletin of Volcanology 76, 1-16.

Blott, S.J., Pye, K., 2001. GRADISTAT: a grain size distribution and statistics package for the analysis of unconsolidated sediments. Earth Surface Processes and Landforms 26, 1237–1248.

Branney, M.J., Kokelaar, P., 2002. Pyroclastic Density Currents and the Sedimentation of Ignimbrites. Geological Society London Memoirs 27, 143 pp.

Breard, E.C.P., Lube, G., 2017. Inside pyroclastic density currents—Uncovering the enigmatic flow structure and transport behaviour in large- scale experiments. Earth and Planetary Science Letters 458, 22–36.

Breard, E.C.P., Jones, J.R., Fullard, L., Lube, G., Davies, C., Dufek, J., 2019. The permeability of volcanic mixtures - Implications for pyroclastic currents. Journal of Geophysical Research, Solid Earth 124. https://doi.org/10.1029/2018JB016544

Brosch, E., Lube, G., 2020. Spatiotemporal sediment transport and deposition processes in experimental dilute pyroclastic density currents. Journal of Volcanology and Geothermal Research 401, 106946. https://doi.org/10.1016/j.jvolgeores.2020.106946.

Cagnoli, B., Romano, G.P., 2010. Effect of grain size on mobility of dry granular flows of angular rock fragments: An experimental determination. Journal of Volcanology and Geothermal Research 193, 18–24.

Calanchi, N., De Rosa, R., Mazzuoli, R., Rossi, P.L., Santacroce, R., Ventura, G., 1993. Silicic magma entering a basaltic magma chamber: eruptive dynamics and magma mixing – an example from Salina (Aeolian Islands, southern Tyrrhenian Sea). Bulletin of Volcanology 55, 504–522.

Cas, R.A.F., Wright, J.V., 1987. Volcanic Successions. Unwin Hyman, London, 528 pp.

Cas, R.A.F., Wright, H.M.N., Folkes, C.B., Lesti, C., Porreca, M., Giordano, G., Viramonte, J.G., 2011. The flow dynamics of an extremely large volume pyroclastic flow, the 2.08-Ma Cerro Galán Ignimbrite, NW Argentina, and comparison with other flow types. Bulletin of Volcanology 73, 1583–1609.

Carey, S.N., 1991. Transport and deposition of tephra by pyroclastic flows and surges. SEPM, Society for Sedimentary Geology, Special Publications 45, 39–57.

Chappell, J., Shackleton, N.J., 1986. Oxygen isotopes and sea level. Nature 324, 137–140.

Chiarabba, C., De Gori, P., Speranza, F., 2008. The Southern Tyrrhenian Subduction Zone: deep geometry, magmatism and Plio-Pleistocene evolution. Earth and Planetary Science Letters 268, 408–423.

Chough, S.K., Sohn, Y.K., 1990. Depositional mechanics and sequences of base surges, Songaksan tuff ring, Cheju Island, Korea. Sedimentology 37, 1115–1135.

Cicchino, A., Zanella, E., De Astis, G., Lanza, R., Lucchi, F., Tranne, C.A., Airoldi, G., Mana S., 2011. Rock magnetism and compositional investigation of Brown Tuffs deposits at Lipari and Vulcano (Aeolian Islands – Italy). Journal of Volcanology and Geothermal Research 208, 23-28.

Cole, P.D., Guest, J.E., Duncan, A.M., 1993. The emplacement of intermediate volume ignimbrite: a case study from Roccamonfina volcano, southern Italy. Bulletin of Volcanology 55, 467–480.

Colella, A., Hiscott, R.N., 1997. Pyroclastic surges of the Pleistocene Monte Guardia sequence (Lipari Island, Italy): depositional processes. Sedimentology 44, 47–66.

Crisci, G.M., De Rosa, R., Lanzafame, G., Mazzuoli, R., Sheridan, M.F., Zuffa, G.G., 1981. Monte Guardia Sequence: a Late-Pleistocene Eruptive Cycle on Lipari (Italy). Bulletin of Volcanology 44, 241-255.

Crisci, G.M., Delibrias, G., De Rosa, R., Mazzuoli, R., Sheridan, M.F., 1983. Age and petrology of the Late-Pleistocene Brown Tuffs on Lipari, Italy. Bulletin of Volcanology 46, 381-391.

Crisci, G.M., De Rosa, R., Esperanca, S., Mazzuoli, R., Sonnino, M., 1991. Temporal evolution of a three component system: the island of Lipari (Aeolian Arc, southern Italy). Bulletin of Volcanology 53, 207-221.

De Astis, G., Dellino, P., De Rosa, R., La Volpe, L., 1997. Eruptive emplacement mechanism of fine grained pyroclastic deposits widespread on Vulcano Island. Bulletin of Volcanology 59, 87-102.

De Astis, G., Ventura, G., Vilardo, G., 2003. Geodynamic significance of the Aeolian volcanism (Southern Tyrrhenian Sea, Italy) in light of structural, seismological and geochemical data. Tectonics 22, 1040–1057.

De Astis, G., Lucchi, F., Dellino, P., La Volpe, L., Tranne, C.A., Frezzotti, M.L., Peccerillo, A., 2013. Geology, volcanic history and petrology of Vulcano (central Aeolian archipelago). Geological Society London, Memoirs 37, 281–348.

De Rosa, R., Donato, P., Gioncada, A., Masetti, M., Santacroce, R. 2003. The Monte Guardia eruption (Lipari, Aeolian Islands): an example of a reversely zoned magma mixing sequence. Bulletin of Volcanology 65, 530–543.

De Rosa, R., Donato, P., Scarciglia, F., 2016. On the origin and post-depositional history of widespread massive ash deposits: the case of Intermediate Brown Tuffs (IBT) of Lipari (Aeolian Islands, Italy). Journal of Volcanology and Geothermal Research 327, 135-151.

Dellino, P., Isaia, R., Veneruso, M., 2004. Turbulent boundary layer shear flows as an approximation of base surge at Campi Flegrei (Southern Italy). Journal of Volcanology and Geothermal Research 133, 211–228.

Dellino, P., Zimanowski, B., Buttner, R., La Volpe, L., Mele, D., Sulpizio, R., 2007. Large-scale experiments on the mechanics of pyroclastic flow: design, engineering, and first results. Journal of Geophysical Research 112, B04202. https://doi.org/10.1029/2006JB004313.

Dellino, P., Buttner, R., Dioguardi, F., Doronzo, D.M., La Volpe, L., Mele, D., Sonder, I., Sulpizio, R., Zimanowski, B., 2010. Experimental evidence links volcanic particle characteristics to pyroclastic flow hazard. Earth and Planetary Science Letters 295, 314–320.

Dellino, P., De Astis, G., La Volpe, L., Mele, D., Sulpizio, R., 2011. Quantitative hazard assessment of phreatomagmatic eruptions at Vulcano (Aeolian Islands, Southern Italy), as obtained by combining stratigraphy, event statistics and physical modelling. Journal of Volcanology and Geothermal Research 201, 264-384.

Dellino, P., Dioguardi, F., Doronzo, D.M., Mele, D., 2019. The rate of sedimentation from turbulent suspension: An experimental model with application to pyroclastic density currents and discussion on the grain-size dependence of flow runout. Sedimentology 66, 129–145.

Douillet, G.A., Taisne, B., Tsang-Hin-Sun, M.S.K., Kueppers, U., Dingwell, D.B., 2015. Syn-eruptive, soft-sediment deformation of deposits from dilute pyroclastic density current: triggers from granular shear, dynamic pore pressure, ballistic impacts and shock waves. Solid Earth 6, 553-572.

Douillet, G.A., Bernard, B., Bouysson, M., Chaffaut, Q., Dingwell, D.B., Gegg, L., Hoelscher, I., Kueppers, U., Mato, C., Ariane Ritz, V., Schlunegger, F., Witting, P., 2019. Pyroclastic dune bedforms: macroscale structures and lateral variations. Examples from the 2006 pyroclastic currents at Tungurahua (Ecuador). Sedimentology 66, 1531-1559.

Druitt, T.H., 1998. Pyroclastic density currents. Geological Society London, Special Publications 145, 145–182.

Druitt, T.H., Avard, G., Bruni, G., Lettieri, P., Maez, F., 2007. Gas retention in fine-grained pyroclastic flow materials at high temperatures. Bulletin of Volcanology 69, 881-901.

Dufek, J., Esposti Ongaro, T., Roche, O., 2015. Pyroclastic density currents: processes and models. In: Sigurdsson, H., Houghton, B., McNutt, S., Rymer, H., Stix, J. (Eds.), The Encyclopedia of Volcanoes (second edition). Academic Press, Elsevier, pp. 631–648.

Ellam, R.M., Menzies, M.A., Hawkesworth, C.J., Leeman, W.P., Rosi, M., Serri, G., 1988. The transition from calc-alkaline to potassic orogenic magmatism in the Aeolian Islands, Southern Italy. Bulletin of Volcanology 50, 386–398.

Farin, M., Mangeney, A., Roche, O., 2014. Fundamental changes of granular flow dynamics, deposition, and erosion processes at high slope angles: insights from laboratory experiments. Journal of Geophysical Research-Earth 119, 504–532.

Félix, G., Thomas, N., 2004. Relation between dry granular flow regimes and morphology of deposits: Formation of levées in pyroclastic deposits. Earth Planetary and Science Letters 221, 197-213.

Folk RL, Ward WC., 1957. Brazos River bar: a study in the significance of grain size parameters. Journal of Sedimentary Petrology 27, 3–26.

Forni, F., Lucchi, F., Peccerillo, A., Tranne, C.A., Rossi, P.L., Frezzotti, M.L., 2013. Stratigraphic and geological evolution of the Lipari volcanic complex (central Aeolian archipelago). Geological Society London Memoirs 37, 213-279.

Francalanci, L., Taylor, S.R., Mcculloch, M.T., Woolhead, J.D., 1993. Geochemical and isotopic variations in the calc-alkaline rocks of Aeolian arc, southern Tyrrhenian Sea, Italy: constraints on magma genesis. Contributions to Mineralogy and Petrology 113, 300–313.

Francalanci, L., Lucchi, F., Keller, J., De Astis, G., Tranne, C.A., 2013. Eruptive, volcano-tectonic and magmatic history of the Stromboli volcano (north-eastern Aeolian archipelago). Geological Society London Memoirs 37, 395–469.Freundt, A., Schmincke, H.U., 1986. Emplacement of small-volume pyroclastic flows at Lacher See (East Eifel, Germany). Bulletin of Volcanology 48, 39–59.

Gase, A., Bradford, J.H., Brand, B., 2018. Estimation of porosity and water saturation in dual porosity pyroclastic deposits from joint analysis of compression, shear, and electromagnetic velocities. Geophysics 83, 1-39.

Giaccio, B., Isaia, R., Fedele, F.G., Di Canzio, E., Hoffecker, J., Ronchitelli, A., Sinitsyn, A.A., Anikovich, M., Lisitsyn, S.N., Popov, V.V., 2008. The Campanian Ignimbrite and Codola tephra layers: Two temporal/stratigraphic markers for the Early Upper Palaeolithic in southern Italy and eastern Europe. Journal of Volcanology and Geothermal Research 177, 208–226.

Gioncada, A., Mazzuoli, R., Bisson, M., Pareschi, M.T., 2003. Petrology of volcanic products younger than 42 ka on the Lipari-Vulcano complex (Aeolian Islands, Italy): an example of volcanism controlled by tectonics. Journal of Volcanology and Geothermal Research 122, 191–220.

Gioncada, A., Mazzuoli, R., Milton, A.J., 2005. Magma mixing at Lipari (Aeolian Islands, Italy): insights from textural and compositional features of phenocrysts. Journal of Volcanology and Geothermal Research 145, 97–118.

Girolami, L., Druitt, T.H., Roche, O., Khrabrykh, Z., 2008. Propagation and hindered settling of laboratory ash flows. Journal of Geophysical Research 113, B02202. http://dx.doi.org/10.1029/2007JB005074.

Goldfarb, D.J., Glasser, B.J., Shinbrot, T., 2002. Shear instabilities in granular flows. Nature 415, 302–305.

Gurioli, L., Cioni, R., Sbrana, A., Zanella, E., 2002. Transport and deposition of pyroclastic density currents over an inhabited area: the deposits of the AD 79 eruption of Vesuvius at Herculaneum, Italy. Sedimentology 49, 1–26.

Hornig-Kjarsgaard, I., Keller, J., Koberski, U., Stadlbauer, E., Francalanci, L., Lenhart, R., 1993. Geology, stratigraphy and volcanological evolution of the island of Stromboli, Aeolian arc, Italy. Acta Vulcanologica 3, 21–68.

Keller, J., 1967. Alter und Abfolge der vulkanischen Ereignisse auf den Aolischen Inseln. Berichte der Naturforschenden Gesellschaft zu Freiburg i. Br. 57, 33–67 (in German).

Keller, J., 1980a. The island of Salina. Rendiconti della Società Italiana di Mineralogia e Petrologia 36, 489-524.

Keller, J., 1980b. The Island of Vulcano. Rendiconti della Società Italiana di Mineralogia e Petrologia 36, 369-414.

Keller, J., Ryan, W.B.F., Ninkovich, D., Altherr, R., 1978. Explosive volcanic activity in the Mediterranean over the past 200 000 yr as recorded in deep-sea sediments. Geological Society of America Bulletin 89, 591–604.

LaBerge, R.D., Giordano, G., Cas, R.A.F., Ailleres, L., 2006. Syn-depositional substrate deformation produced by the shear force of a pyroclastic density current: An example from the Pleistocene ignimbrite at Monte Cimino, northern Lazio, Italy. Journal of Volcanology and Geothermal Research 158, 307–320.

Leocat, E., 2011. Histoire Eruptive des Volcans du Secteur Occidental des Iles Eoliennes (Sud de la Mer Tyrrhenienne, Italie) (Ph.D. thesis). University of Paris 11, Orsay (in French and English).

Losito, R., 1989. Stratigrafia, Caratteri Deposizionali e Aree Sorgente dei Tufi Bruni delle Isole Eolie (Ph.D. thesis). University of Bari, Italy (in Italian).

Lowe, D.R., 1982. Sediment gravity flows: II. Depositional models with special references to deposits of high-density turbidity currents. Journal of Sedimentary Petrology 52, 279–297.

Lube, G., Cronin, S.J., Platz, T., Freundt, A., Procter, J.N., Henderson, C., Sheridan, M.F., 2007. Flow and deposition of pyroclastic granular flows: a type example from the 1975 Ngauruhoe eruption, New Zealand. Journal of Volcanology and Geothermal Research 161, 165–186.

Lube, G., Breard, E.C.P., Jones, J., Fullard, L., Dufek, J., Cronin, S.J., Wang, T., 2019. Generation of air lubrication within pyroclastic density currents. Nature Geoscience 12, 381-386.

Lube, G., Breard, E.C.P., Esposti-Ongaro, T., Dufek, J., Brand, B., 2020. Multiphase flow behaviour and hazard prediction of pyroclastic density currents. Nature Reviews Earth & Environment 1, 348-365.

Lucchi, F., 2009. Late-Quaternary marine terrace deposits as tools for wide-scale correlation of unconformity-bounded units in the volcanic Aeolian archipelago (southern Italy). Sedimentary Geology 216, 158–178.

Lucchi, F., 2013. Stratigraphic methodology for the geological mapping of volcanic areas: insights from the Aeolian archipelago (southern Italy). Geological Society London Memoirs 37, 37–55.

Lucchi, F., Tranne, C.A. Calanchi, N., Pirazzoli, P.A., Romagnoli, C., Radtke, U., Reyss, J.L., Rossi, P.L., 2004. Stratigraphic constraints to date late-Quaternary ancient shorelines and to evaluate vertical movements at Lipari (Aeolian Islands). Quaternary International 115/116, 105–115.

Lucchi, F., Tranne, C.A., De Astis, G., Keller, J., Losito, R., Morche, W., 2008. Stratigraphy and significance of Brown Tuffs on the Aeolian Islands (southern Italy). Journal of Volcanology and Geothermal Research 177, 49-70.

Lucchi, F., Gertisser, R., Keller, J., Forni, F., De Astis, G., Tranne, C.A., 2013a. Eruptive history and magmatic evolution of the island of Salina (central Aeolian archipelago). Geological Society London Memoirs 37, 155-211.

Lucchi, F., Keller, J., Tranne, C., 2013b. Regional stratigraphic correlations across the Aeolian archipelago (southern Italy). Geological Society London Memoirs 37, 55-81.

Lucchi, F., Tranne, C.A., Peccerillo, A., Keller, J., Rossi, P.L., 2013c. Geological history of the Panarea volcanic group (eastern Aeolian archipelago). Geological Society London Memoirs 37, 349-393.

Lucchi, F., Peccerillo, A., Tranne, C.A., Rossi, P.L., Frezzotti, M.L., Donati, C., 2013d. Volcanism, calderas, and magmas of the Alicudi composite volcano (western Aeolian archipelago). Geological Society London Memoirs 37, 83–111.

Lucchi, F., Santo, A.P., Tranne, C.A., Peccerillo, A., Keller, J., 2013e. Volcanism, magmatism, volcano-tectonics and sea-level fluctuations in the geological history of Filicudi (western Aeolian archipelago). Geological Society London Memoirs 37, 113-153.

Mangeney, A., Roche, O., Hungr, O., Mangold, N., Faccanoni, G., Lucas, A., 2010. Erosion and mobility in granular collapse over sloping beds, Journal of Geophysical Research-Earth 115, F03040. https://doi.org/10.1029/2009JF001462.

Manetti, P., Pasquaré, G., Tibaldi, A., Tsegaye, A., 1988. Geology of the island of Filicudi (Aeolian arc). Bollettino G.N.V. (Gruppo Nazionale di Vulcanologia, Italia) IV, 368-382.

Manetti, P., Pasquaré, G., Tibaldi, A., Tsegaye, A., 1995. A new geo-vulcanological map of Filicudi island (Aeolian arc, Italy). Acta Vulcanologica 7, 1-5.

Mathisen, M.E., Vondra, C.F., 1983. The fluvial and pyroclastic deposits of the Cagayan basin, Northern Luzon, Philippines—an example of non-marine volcaniclastic sedimentation in an interarc basin. Sedimentology 30, 369–392.

Mele, D., Dioguardi, F., Dellino, P., Isaia, R., Sulpizio, R., Braia, G., 2015. Hazard of pyroclastic density currents at the Campi Flegrei Caldera (Southern Italy) as deduced fromthe combined use of facies architecture, physical modeling and statistics of the impact parameters. Journal of Volcanology and Geothermal Research 299, 35–53.

Meschiari, S., Albert, P.G., Lucchi, F., Sulpizio, R., Smith, V.C., Kearne, R., Tranne, C.A., 2020. Frequent activity on Vulcano (Italy) spanning the last 80 ky: New insights from the chemo-stratigraphy of the Brown Tuffs. Journal of Volcanology and Geothermal Research 406. https://doi.org/10.1016/ j.jvolgeores.2020.107079.

Miall, A.D., 1978. Lithofacies types and vertical profiles models in braided river deposits: a summary. In: Miall, A.D. (Ed.), Fluvial Sedimentology. Canadian Society of Petroleoum Geologists, Memoirs 5, 597–604.

Miall, A.D., 1985. Architectural-element analyses: a new method of facies analyses applied to fluvial deposits. Earth-Science Reviews 22, 261–308.

Mills, P.C., 1983. Genesis and diagnostic value of soft-sediment deformation structures: a review. Sedimentary Geology 35, 83–104.

Morche, W., 1988. Tephrochronologie der Aolischen Inseln (Ph.D. thesis). Albert-Ludwigs-Universitat Freiburg, Germany (in German).

Nichols, R., Sparks, R., and Wilson, C., 1994. Experimental studies of the fluidization of layered sediments and the formation of fluid escape structures. Sedimentology 41, 233–253.

Odonne, F., Callot, P., Debroas, E.-J., Sempere, T., Hoareau, G., and Maillard, A., 2011. Soft-sediment deformation from submarine sliding: Favourable conditions and triggering mechanisms in examples from the Eocene Sobrarbe delta (Ainsa, Spanish Pyrenees) and the mid-Cretaceous Ayabacas Formation (Andes of Peru). Sedimentary Geology 235, 234–248.

Owen, G., 1987. Deformation processes in unconsolidated sands. Geological Society London, Special Publications 29, 11–24.

Peccerillo, A., De Astis, G., Faraone, D., Forni, F., Frezzotti, M.L., 2013. Compositional variations of magmas in the Aeolian arc: implications for petrogenesis and geodynamics. Geological Society London, Memoirs 37, 489–508.

Pichler, H., 1980. The Island of Lipari. Rendiconti della Società Italiana di Mineralogia e Petrologia 36, 415-440.

Pollock, N.M., Brand, B.D., Rowley, P.J., Sarocchi, D., Sulpizio, R., 2019. Inferring pyroclastic density current flow conditions using syn-depositional sedimentary structures. Bulletin of Volcanology 81, 46. http://dx.doi.org/10.1007%2Fs00445-019-1303-z

Kowalczuk, P.B., Drzymala, J., 2016. Physical meaning of the Sauter mean diameter of spherical particulate matter. Particulate Science and Technology 34, 645-647.

Roche, O, 2015. Nature and velocity of pyroclastic density currents inferred from models of entrainment of substrate lithic clasts. Earth Planetary and Science Letters 418, 115-125.

Roche, O., Montserrat, S., Niño, Y., Tamburrino, A., 2008. Experimental observations of water-like behaviour of initially fluidized, unsteady dense granular flows and their relevance for the propagation of pyroclastic flows. Journal of Geophysical Research 113, B12203. http://dx.doi.org/10.1029/2008JB 005664.

Roche, O., Niño, Y., Mangeney, A., Brand, B.D., Pollock, N.M., Valentine, G.A., 2013. Dynamic pore-pressure variations induce substrate erosion by pyroclastic flows. Geology 41, 1107–1110.

Roche, O., Buesch, D.C., Valentine, G.A., 2016. Slow-moving and far-travelled dense pyroclastic flows during the Peach Spring super-eruption. Nature Communications 7, 10890. doi: 10.1038/ncomms10890

Roche, O., Azzaoui, N., Guillin, A., 2021. Discharge rate of explosive volcanic eruption controls runout distance of pyroclastic density currents. Earth and Planetary Science Letters 568, 117017. https://doi.org/10.1016/j.epsl.2021.117017

Røe, S.-L., Hermansen, M., 2006. New aspects of deformed cross-strata in fluvial sandstones: examples from Neoproterozoic formations in northern Norway. Sedimentary Geology 186, 283–293.

Rohling, E.J., Foster, G.L., Grant, K.M., Marino, G., Roberts, A.P., Tamisiea, M.E., Williams, F., 2014. Sea-level and deep-sea-temperature variability over the past 5.3 million years. Nature 508, 477–482.

Rowley, P.J., Kokelaar, P., Menzies, M., Waltham, D., 2011. Shear derived mixing in dense granular flows. Journal of Sedimentary Research 81, 874–884.

Sauter, J., 1926. Die Grössenbestimmung der in Gemischnebeln von Verbrennungskraftmaschinen vorhandenen Brennstoffteilchen. VDI-Verlag, Berlin, Forschungsarbeiten auf dem Gebiete des Ingenieurwesens, 279 pp (in German).

Selker, J.S., 1993. Expressions for the formation of load casts in soft sediment. Journal of Sedimentary Research 63, 1149–1151.

Smith, G.A., 1986. Coarse-grained nonmarine volcaniclastic sediment: terminology and depositional process. Geological Society of America Bulletin 97, 1–10.

Smith, G.A., 1987. The influence of explosive volcanism on fluvial sedimentation: the Deschutes formation (Neogene) in central Oregon. Journal of Sedimentary Petrology 57, 613–629.

Smith, G.M., Williams, R., Rowley, P.J., Parsons, P.D., 2018. Investigation of variable aeration of monodisperse mixtures: implications for pyroclastic density currents. Bulletin of Volcanology 80, 67. https://doi.org/10.1007/s00445-018-1241-1

Sohn, Y.K., Chough, S.K., 1989. Depositional processes of the Suwolbong Tuff Ring, Cheju Island (Korea). Sedimentology 36, 837–855.

Sohn, Y.K., 1997. On traction carpet sedimentation. Journal of Sedimentary Research 67, 502–509.

Sulpizio, R., Dellino, P., 2008. Sedimentology, depositional mechanisms and pulsating behaviour of pyroclastic density currents. Developments in Volcanology 10, 57–96.

Sulpizio, R., Mele, D., Dellino, P., La Volpe, L., 2007. Deposits and physical properties of pyroclastic density currents during complex Subplinian eruptions: the AD 472 (Pollena) eruption of Somma-Vesuvius, Italy. Sedimentology 54, 607–635.

Sulpizio, R., De Rosa, R., Donato, P., 2008a. The influence of variable topography on the depositional behaviour of pyroclastic density currents: the examples of the Upper Pollara eruption (The island of Salina, southern Italy). Journal of Volcanology and Geothermal Research 175, 367–385.

Sulpizio, R., Bonasia, R., Dellino, P., Di Vito, M.A., La Volpe, L., Mele, D., Zanchetta, G., Sadori, L., 2008b. Discriminating the-long distance dispersal of fine ash from sustained columns or near ground ash clouds: the example of the Pomici di Avellino eruption (Somma-Vesuvius, Italy). Journal of Volcanology and Geothermal Research, 177, 263-276. doi: 10.1016/j.jvolgeores.2007.11.012

Sulpizio, R., Bonasia, R., Dellino, P., Mele, D., Di Vito, M.A., La Volpe, L., 2010. The Pomici di Avellino eruption of Somma-Vesuvius (3.9 ka BP). Part II: Sedimentology and physical volcanology of pyroclastic density current deposits. Bulletin of Volcanology 72, 559–577.

Sulpizio, R., Alçiçek, M.C., Zanchetta, G., Solari, L., 2013. Recognition of the Minoan tephra in Acigöl Basin, Western Turkey: implications for inter archive correlations and fine ash dispe. Journal of Quaternary Science, 28, 329-336.

Sulpizio, R., Dellino, P., Doronzo, D.M., Sarocchi D., 2014. Pyroclastic density currents: state of the art and perspectives. Journal of Volcanology and Geothermal Research 283, 36–65.

Sulpizio, R., Castioni, D., Rodriguez-Sedano, L.A., Sarocchi, D., Lucchi, F., 2016. The influence of slope-angle ratio on the dynamics of granular flows: insights from laboratory experiments. Bulletin of Volcanology 78, 77. https://doi.org/10.1007/s00445-016-1069-5

Tomlinson, E.L., Albert, P.G., Wulf, S., Brown, R., Smith, V.C., Keller, J., Orsi, G., Bourne, A.J., Menzies, M.A., 2014. Age and geochemistry of tephra layers from Ischia, Italy: constraints from proximal-distal correlations with Lago Grande di Monticchio. Journal of Volcanology and Geothermal Research 287, 22-39.

Valentine, G.A., 1987. Stratified flow in pyroclastic surges. Bulletin of Volcanology 49, 616–630.

Valentine, G.A., Buesch, D.C., Fisher, R.V., 1989. Basal layered deposits of the Peach Springs Tuff, northwestern Arizona, USA. Bulletin of Volcanology 51, 395–414.

Ventura, G., 2013. Kinematics of the Aeolian volcanism (Southern Tyrrhenian Sea) from geophysical and geological data. Geological Society London, Memoirs 37, 3–11.

Waelbroeck, C., Labeyrie, L., Michel, E., Duplessy, J.C., McManus, J.F., Lambeck, K., Balbon, E., Labracherie, M., 2002. Sea-level and deep water temperature changes derived from foraminifera isotopic records. Quaternary Science Reviews 21, 295–305.

Waresback, D.B., Turbeville, B.N., 1990. Evolution of a Plio-Pleistocene volcanogenic alluvial fan: the Puye formation, Jemez Mountains, New Mexico. Geological Society America Bulletin 102, 298–314.

TABLES

Tab. 1. Selected outcrops, stratigraphy and measurements of the sin-depositional sedimentary structures. The distance from the source area is arbitrarily measured relative to the centre of the La Fossa Caldera. The sample names refer to the BT depositional units selected for chemical analyses. Labels for the sedimentary structures: MB=mixing band; US=undulated structure; FS=recumbent flame structure; RS=rip-up structure. In the column of sedimentary structures, the symbol / indicates that there is no direct evidence in the field of mixed lithofacies, but the process of clast-embedding is outlined by means of geochemical analyses.

Tab. 2. Lithofacies codes, description and interpretation of the lithofacies recognised in the BT investigated in the present work. The first letters of the lithofacies code indicate the general appearance of the deposit (m = massive, ps = planar stratified, xs = cross-stratified, is = intermittently stratified, etc.) and the capital letters indicate the grain size (A = ash, L = lapilli).

Tab. 3. Grain size statistical parameters of Folk and Ward (1957) for the different sub-populations recognised in the samples from the base of some BT depositional units: BT=Brown Tuffs; mg=Monte Guardia unit; lpt=Lower Pollara Tuffs; fa=Falcone unit. The parameters by Folk and Ward (1957) were calculated by means of the GRADISTAT program (Blott and Pye, 2001). The Sauter mean diameter (Sauter 1926) of the different BT sub-populations is estimated using the method of Breard et al. (2019).

FIGURES

Fig. 1. Sketch maps of the islands of Vulcano and Lipari (A) showing the areal distribution of the BT deposits and the location of outcrops where the sedimentary structures object of the present study have been observed (L1-13, V1-6). The inset (B) shows the location of the Aeolian Islands and seamounts in the southern Tyrrhenian sea (depth contour lines in metres below sea level). Coordinates conform to the Gauss-Boaga System (IGM). In (C) there is a sketch chronostratigraphic framework showing the development of Aeolian subaerial volcanism and the time-stratigraphic interval of BT deposition. Labels for the main tephra layers are: pt = Petrazza Tuffs; gpt = Grey Porri Tuffs; it = Ischia Tephra; lpt = Lower Pollara Tuffs; gu = Monte Guardia pumice; vg = Vallone del Gabellotto pumice; pn = Punte Nere tuffs. References: Alicudi = Lucchi et al. (2013c); Filicudi = Lucchi et al. (2013d); Salina = Lucchi et al. (2013a); Lipari = Forni et al. (2013); Panarea = Lucchi et al. (2013b); Vulcano = De Astis et al. (2013); Stromboli = Francalanci et al. (2013).

Fig. 2. Generalized stratigraphic succession of the BT derived from correlations between the islands of Lipari and Vulcano. The BT succession is subdivided into (at least) 16 depositional units (BT1-

16) superposed to the LBT, IBT, IBT-upper and UBT macro-units by means of interlayered volcanic units and tephra layers, erosive surfaces and reworked horizons (see also Meschiari et al., 2020). The individual depositional units of the UBT on Vulcano have a different name because they cannot be directly correlated with those on Lipari. References for the stratigraphy of the two islands are: Forni et al., 2013 (Lipari); De Astis et al., 2013 (Vulcano). The stratigraphic units interlayered within the BT that are characterised by the sedimentary structures object of this work are described in Table 1.

Fig. 3. Outcrop photographs of the BT and their distinctive lithofacies. A) Massive deposits (lithofacies mA) of the BT on Lipari (outcrop L5). The BT in this outcrop correspond to the IBT-upper and UBT macro-units developed above the Monte Guardia marker bed. B) UBT deposits on Vulcano (outcrop V1) characterised by planar to cross-stratified lithofacies (psA-xsA). C) Alternating massive (mA) and intermittently stratified (isA) lithofacies of the UBT on Vulcano (outcrop V3). D) Detailed view of the deposits of Figure 3C. E) Detail of the ruptured laminae of the intermittently stratified deposits of UBT. The arrows indicate distinctive upward bending of the laminae in the rupture points. F) Intermittently stratified ash (isA) deposits of the UBT on Vulcano (outcrop V2). G) Close view of the deposits of Figure 3G showing ruptured laminae with typical upward deformation and columns of coarse ash (arrow) and inflated deformation of the laminae before the rupture (*). H) Close view of the deposits of Figure 3G showing ruptured laminae with typical upward deformation (arrow). I) Massive deposits of the UBT on Vulcano near to Grotta dei Pisani that contain fragments of laminae (arrows) representing relicts of the stratified lithofacies.

Fig. 4. Field evidence of the mixing bands recognised at base of different BT depositional units on Lipari and Vulcano, shown in stratigraphic order (starting from the oldest) according to Fig. 2. A) Vallone dei Lacci, Lipari (outcrop L8): mixing band (*) between the BT4 depositional unit and the Grey Porri Tuffs (gpt). B) Valle Muria, Lipari (outcrop L2): mixing band (*) between the BT8 depositional unit and the Punta del Perciato pumice (pe). C) Mixing band (*) between the BT9

depositional unit and the Falcone pumice (pe) at Valle Muria, Lipari (outcrop L2). D) Detail of the mixing band in Figure 4C. E) Spiaggia Valle Muria, Lipari (outcrop L1): mixing band (*) between the BT9 depositional unit and the Falcone pumice (pe). F) Valle Muria, Lipari (outcrop L2): scattered pumice lapilli of the Falcone unit (fa) embedded within the overlying BT9 depositional unit. G) Gelso, Vulcano (outcrop V5): mixing band (*) between the BT12 depositional unit and the Monte Guardia tephra layer (gu). H) Passo del Piano, Vulcano (outcrop V1): mixing band (*) between the BT16(V) depositional unit and the Vallone del Gabellotto pumice (vg).

Fig. 5. Field evidence of shear structures on Lipari. A) Tunnel Canneto, Lipari (outcrop L5): undulated structure (lithofacies ucAL) along the contact between the BT12 depositional unit and the underlying Monte Guardia pumice succession. B) Crest of the undulated structure of Figure 5A. In the inset it is shown a zoom on the crest of the undulated structure made up of mixed material between the BT12 and the underlying incoherent pyroclastic deposit. C) Spiaggia Valle Muria, Lipari (outcrop L1): panoramic view of the undulated structure (lithofacies ucAL) along the contact between the BT9 depositional unit and the underlying Falcone pumice succession. D) Trail of pumice and lithic lapilli of the Falcone pumice succession embedded within the overlying BT9 depositional unit (see C for location), representing the tail of a recumbent flame structure (lithofacies rfAL). E) Deformed bed of mixed material between the BT9 depositional unit and pumice lapilli from the underlying Falcone succession, representing the trunk of a not fully developed recumbent flame structure (lithofacies rfAL). F) Detail of the undulated contact in Figure 5C showing a hook-like structure of rip-up lapilli from the underlying Falcone unit (lithofacies ruAL).

Fig. 6. Grain-size and components frequency histograms of weight % at half-phi intervals and pie charts of the components of representative samples of the mixing bands at the base of distinct BT depositional units in outcrops L2, L5, L10 and L12 on Lipari (see Fig. 1A for location).

Representative photographs of the outcrops are also shown. The outcrops are displayed relative to an increasing distance from the inferred source area of La Fossa Caldera on Vulcano from base to top.

Fig. 7. TAS (A) and K_2O/SiO_2 (B) classification diagrams of the BT glasses compared to the volcanic glasses of explosive eruption deposits produced on Vulcano, Lipari and Salina during the last 50 ky. Data for the BT glasses are from Meschiari et al. (2020), whislt the data for Vulcano, Lipari and Salina are from Albert et al. (2017). Error bars represent 2*standard deviations of replicated analyses of the StHs6/80-G secondary standard glass run alongside the BT samples. The secondary components recognised in distinct BT depositional units referred to the LBT, IBT, IBT-upper and UBT macro-units are compared to the compositions of the underlying proximal pyroclastic units in distinct major element glass geochemical variation diagrams (A-N). The stratigraphic succession of BT depositional units (BT3, BT4, BT8, BT9, BT10, BT12, BT14-V, BT16-V) refers to Fig. 2. Data for the BT glasses are from Meschiari et al. (2020). References for the pyroclastic units used for comparison are: Grey Porri Tuffs (w.r.) = Sulpizio et al. (2016); Grey Porri Tuffs, Salina, proximal = Albert et al. (2017); Grey Porri Tuffs, Lipari medial, Vulcano medial-distal and Panarea, distal = Sulpizio et al., 2016; Meschiari et al. (2020); Lip1 = Meschiari et al. (2020); Falcone = Albert et al. (2017); Punta del Perciato = Albert et al. (2017); Monte Guardia field = Albert et al. (2017) and Meschiari et al. (2020); Monte Guardia (1) = Albert et al. (2017); Monte Guardia (2) = Meschiari et al. (2020); Cugni di Molinello = Meschiari et al. (2020); Vallone del Gabellotto (1) = Albert et al. (2017); Vallone del Gabellotto (2) = Meschiari et al. (2020).

Fig. 8. Sketch of the transport and depositional behaviour of the PDCs during the UBT eruptions on Vulcano island when interacting with the La Fossa Caldera wall (arrows indicate the flow direction). In the inbox, a model explaining the formation of lithofacies altpsmA (alternance of planar stratified and massive ash) as continuous aggradation of deposits from different PDC pulses (a, b, c, d) in the area of il Piano to the south of the source area, and the lithofacies isA

(intermittently stratified ash) as disruption of the deposits due to fluid escape (d, e, f). Not to scale.

Fig. 9. Sketch of the formation of syn-depositional sedimentary structures (mixing bands, undulated structures and recumbent flame structures) at the base of the BT deposits as the result of lateral transport and high shear stress exerted by the PDCs of the BT on the loose underlying pyroclastic (pumice) material along downslope and upslope paths on the island of Lipari, to the north of the La Fossa Caldera source area. Arrows indicate the flow direction. Not to scale.

Fig. 10. Sketch of the transport and depositional behaviour of the BT PDCs laterally spreading from the La Fossa caldera source on Vulcano towards the island of Lipari, crossing the narrow sea arm of the Bocche di Vulcano and interacting with the irregular paleo-topography of Lipari (see explanation in the text).

Fig. 11. Diagrams showing variations of minimum basal shear velocity (u_*) vs. relative flow concentration between PDCs and an underlying bed ($\boldsymbol{x} = \rho_{PDC} / \rho_{bed}$) for different wavelength numbers ($\lambda/2\pi$) of basal instabilities. Dashed lines indicate the minimum basal shear velocity for the observed wavelength of undulated structures of 40 cm ($\lambda/2\pi$=0.16) and 450 cm ($\lambda/2\pi$=0.72 as example of bed instabilities in the case study of the BT eruptions.

SUPPLEMENTARY MATERIAL

Supplementary File 1 - Main characteristics of tephra units used for the subdivisions of the BT succession and showing evidence of syn-depositional clast incorporation within distinct BT depositional units (listed in stratigraphic order starting from the older one). Chemical composition of juvenile glass fragments (w.r=whole rock) and mineralogy are reported by referring to: (1) present work; (2) Meschiari et al. (2020); (3) Albert et al (2017); (4) Sulpizio et al. (2016); (5) Tomlinson et al. (2014); (6) De Astis et al (2013); (7) Gioncada et al. (2005); (8) De Rosa et al. (2003); (9) Calanchi et al. (1993). Labels for compositions: CA=calcalkaline, HKCA=high-k calcalkaline, SHO=shoshonite series; Bas-And=basaltic andesite, And=andesite, Dac=dacite, Rhy=rhyolite, Sho=shoshonite. Labels for phenocrysts: pl=plagioclase, kf=K-feldspar; cpx=clinopyroxene; opx=orthopyroxene, bt=biotite; ol=olivine; amp=amphibole; ox=oxides; ap=apatite; zr=zircon; ti=titanite; acm=acmite). Proximal stratigraphic units refer to: (1) Lucchi et al. (2008); (2) Forni et al. (2013); (3) Lucchi et al. (2013a); (4) De Astis et al. (2013). Age references: (1) Morche (1988); (2) Soligo et al. (2000); (3) Siani et al. (2004); (4) Leocat (2011); (5) Lucchi et al. (2013a; 2013b); (6) Sulpizio et al. (2016); (7) Giaccio et al. (2017); (8) Meschiari et al. (2020).

Supplementary File 2 - Representative major and minor element compositions of samples relative to the mixing bands recognised in this study at the base of different Brown Tuffs (BT) units, according to LBT, IBT, IBT-upper and UBT macro-units. Totals are pre-normalised analytical totals. For each of the samples, we include representative analyses for the main BT juvenile component and the secondary components (sec. comp.) relative to the process of clast embedding from the underlying pyroclastic units. Representative analyses for the proximal pyroclastic units used for the correlation of the secondary components are reported for comparison (in grey): gpt=Grey Porri Tuffs, Salina; pe=Punta del Perciato, Lipari; fa=Falcone, Lipari; Lip1 tephra layer, Lipari; mg=Monte Guardia, Lipari; cm=Cugni di Molinello, Vulcano; vg=Vallone del Gabellotto, Lipari. Compositions of the proximal pyroclastic units and the BT conform to Meschiari et al. (2020), except for "pe", "fa" and "mg" which are from Albert et al. (2017).

Highlights

- Sedimentological analysis of widespread ash-rich pyroclastic deposits
- Deposits from ground-hugging pulsating pyroclastic density currents (PDCs)
- Post-depositional disruption due to fluid escape and dissipation of pore pressure
- Erosion and clast embedding by PDCs at several kms away from the source area
- Shear-related granular instability structures at the base of PDC deposits

Figure 1 Click here to access/download;Figure;Fig. 1_lucchi.jpg

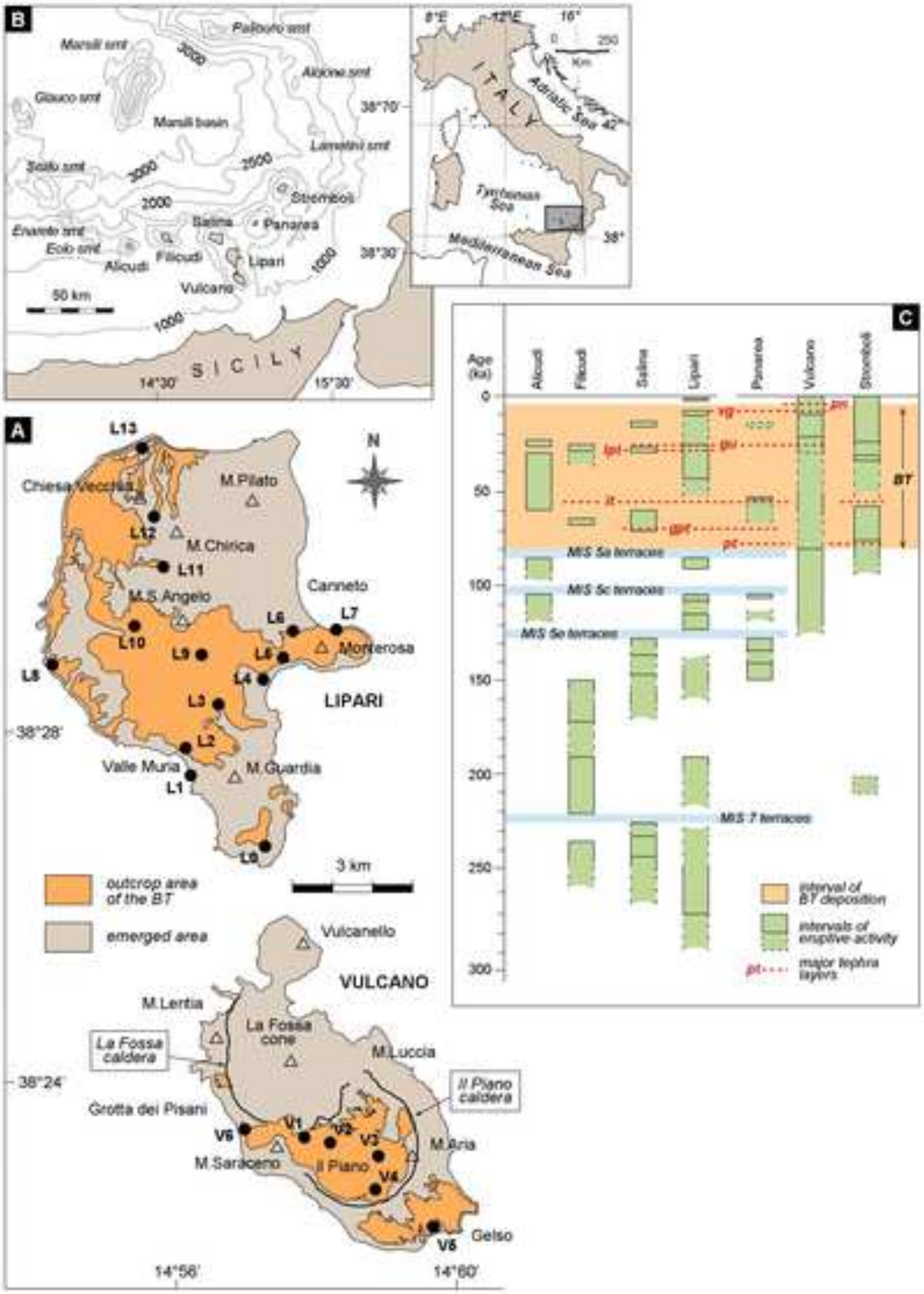

Fig. 1

Figure 2

Click here to access/download;Figure;fig. 2_lucchi.jpg

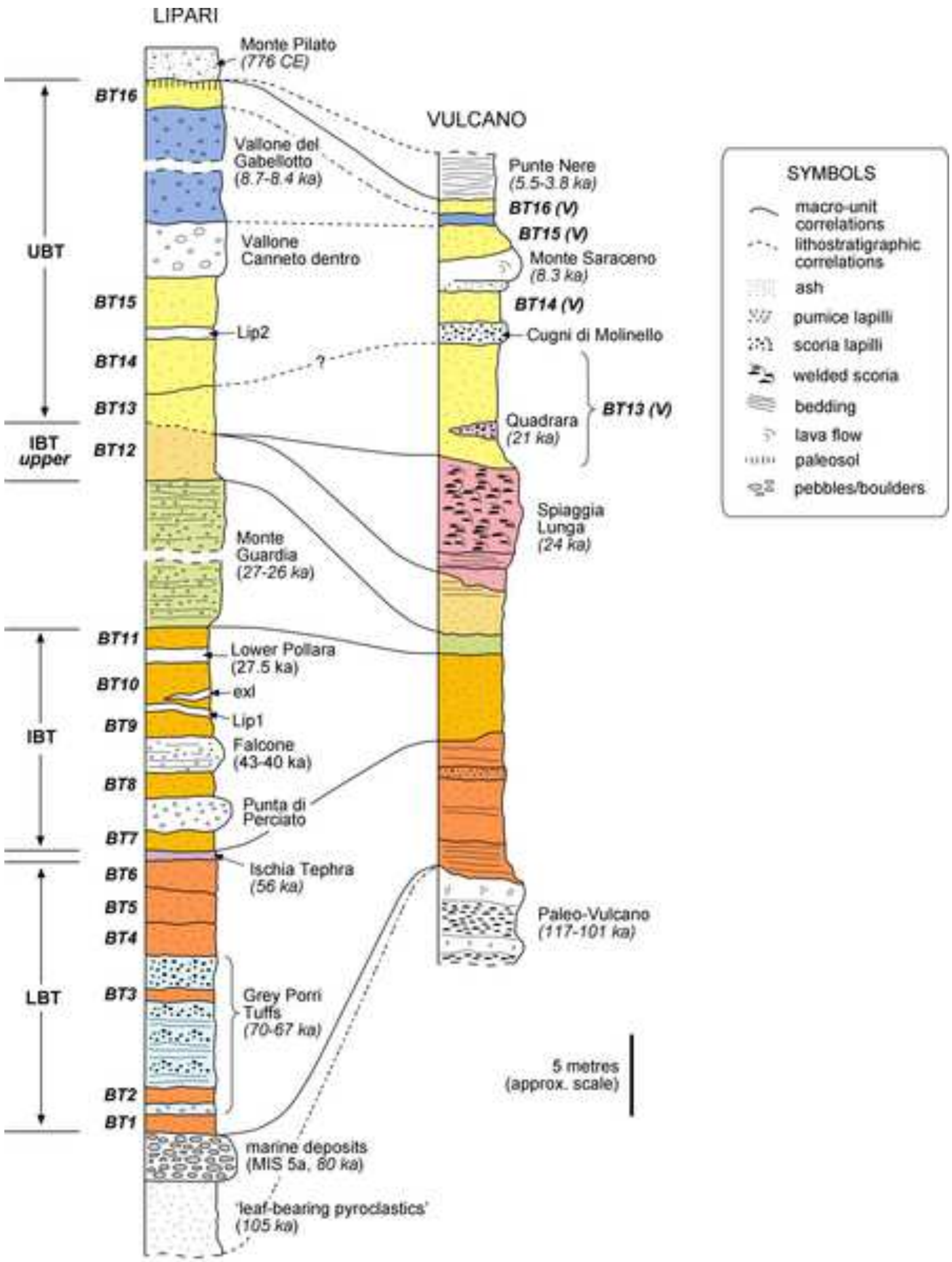

Fig. 2

Figure 3

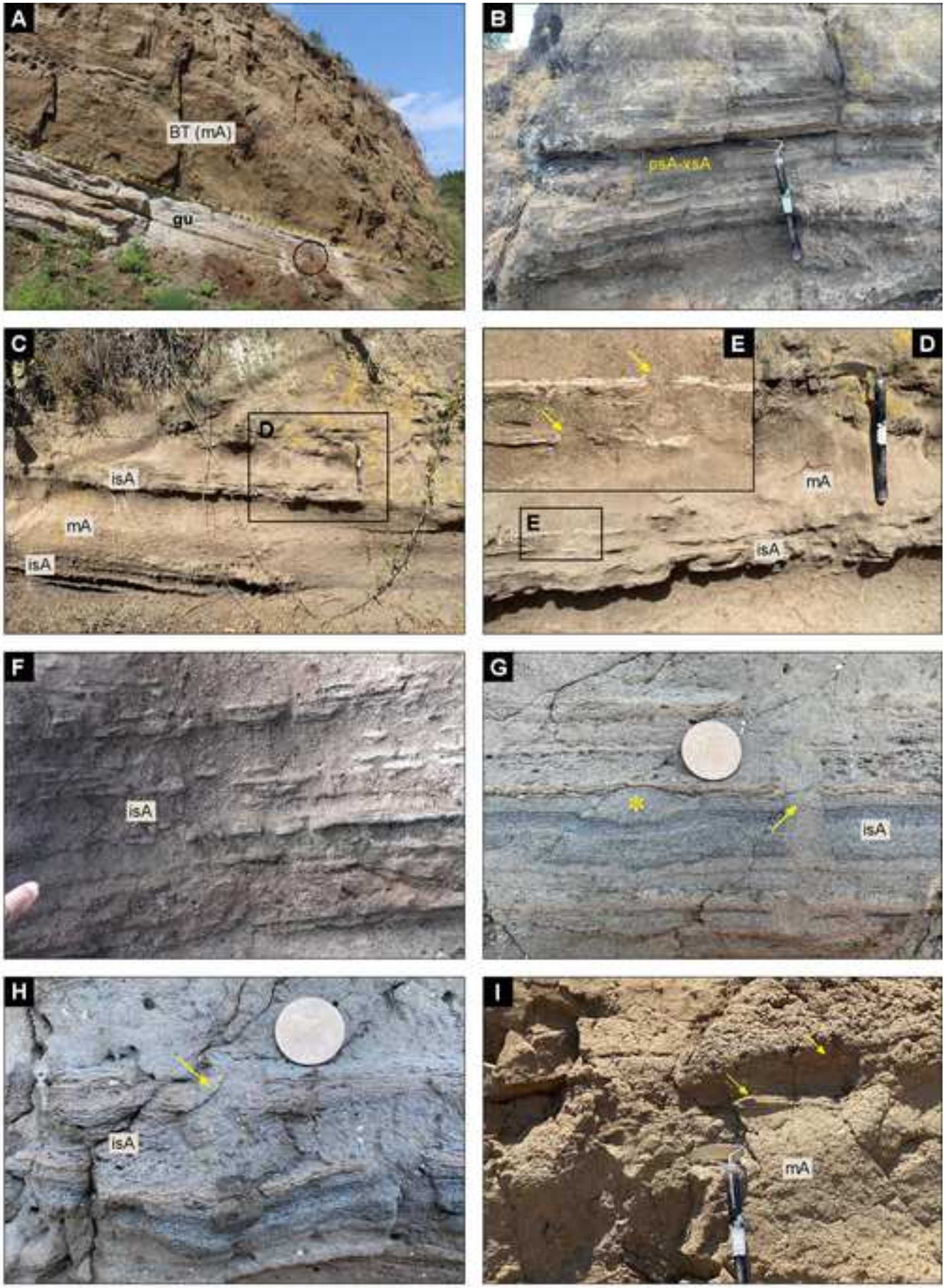

Fig. 3

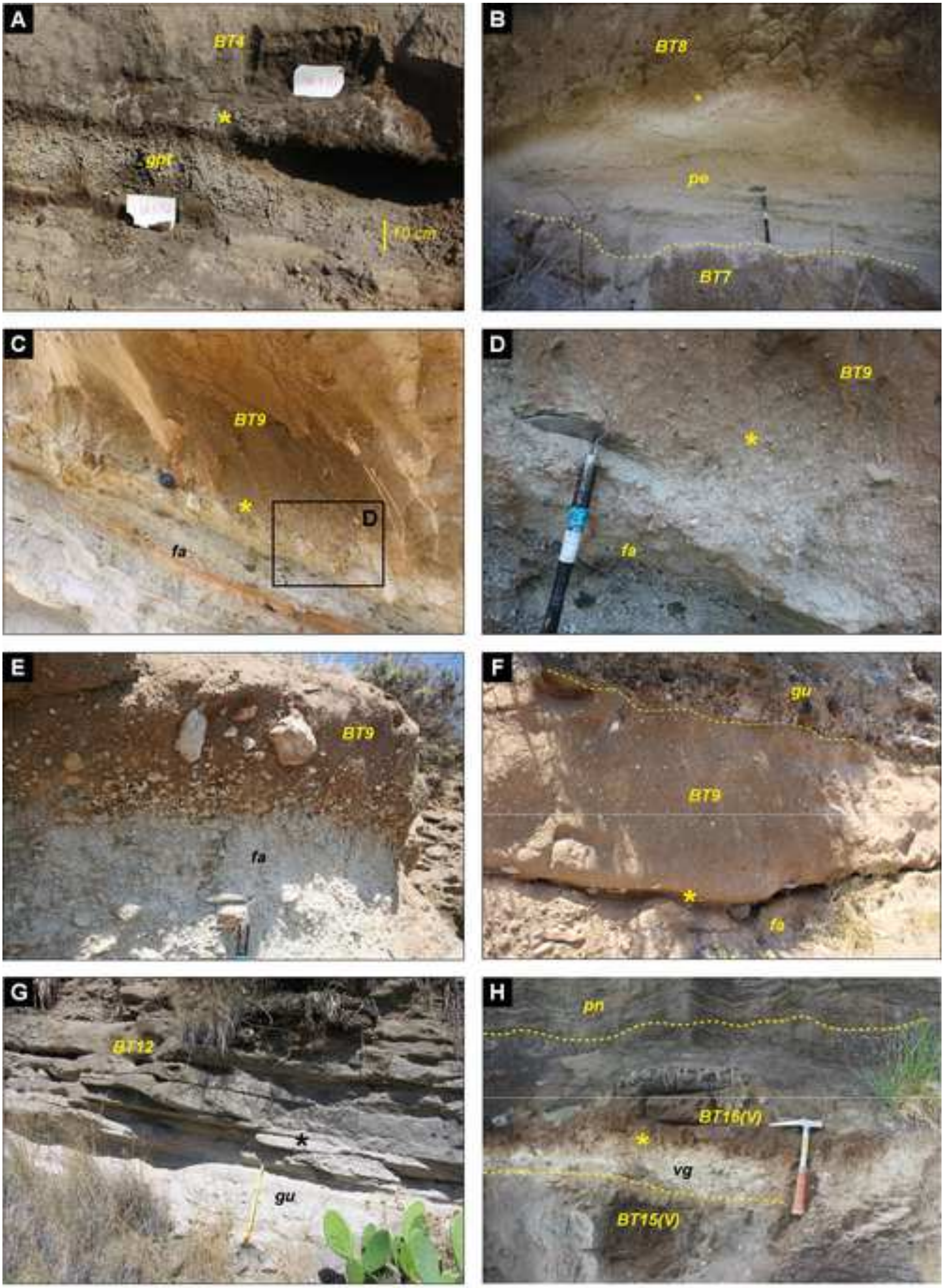
A
BT4
gpt
10 cm
B
BT8
pe
BT7
C
BT9
fa
D
BT9
fa
E
BT9
fa
F
gu
BT9
fa
G
BT12
gu
H
pn
BT16(V)
vg
BT15(V)

Fig. 4

Figure 5 Click here to access/download;Figure;fig. 5_lucchi.jpg

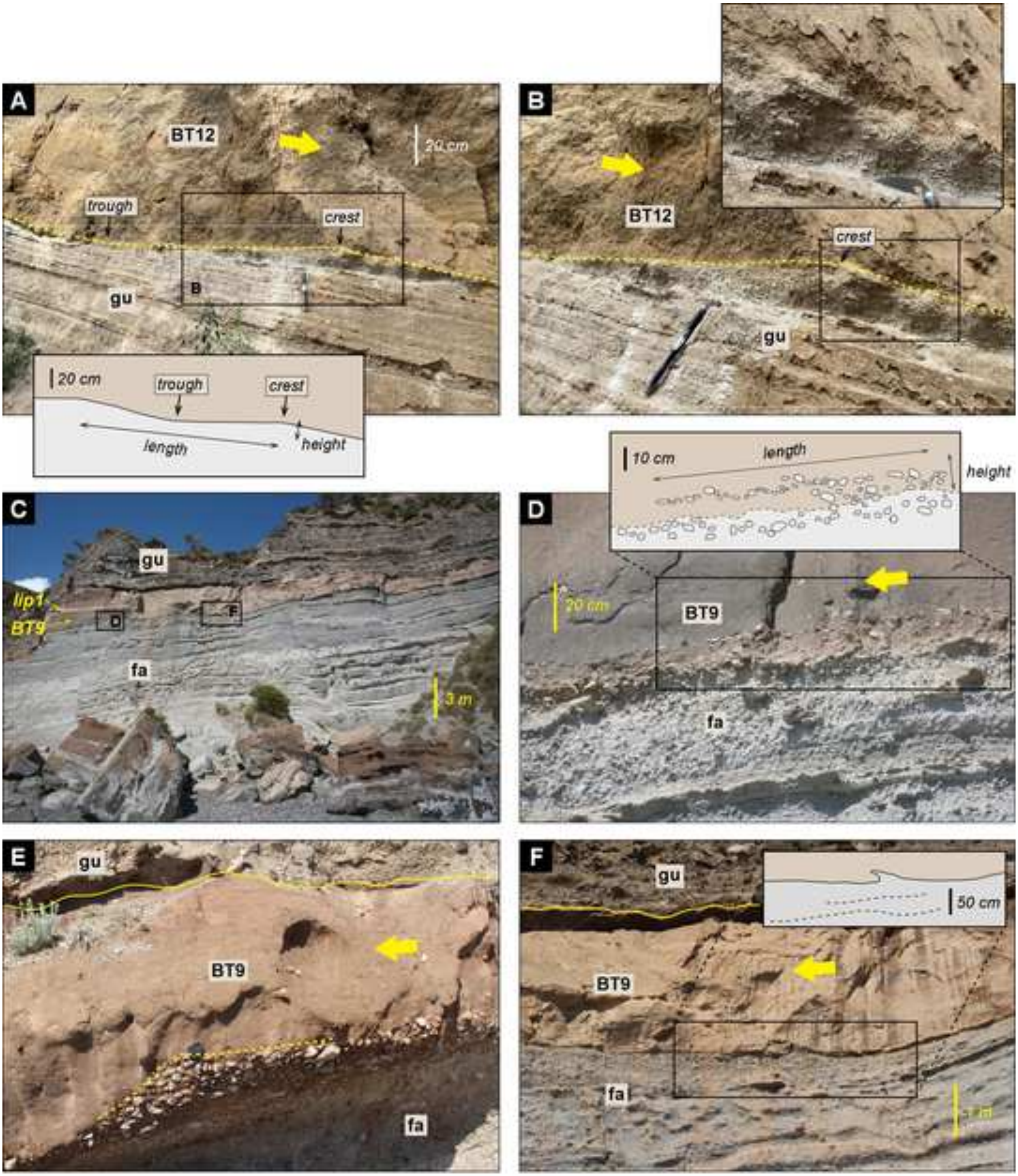

Fig. 5

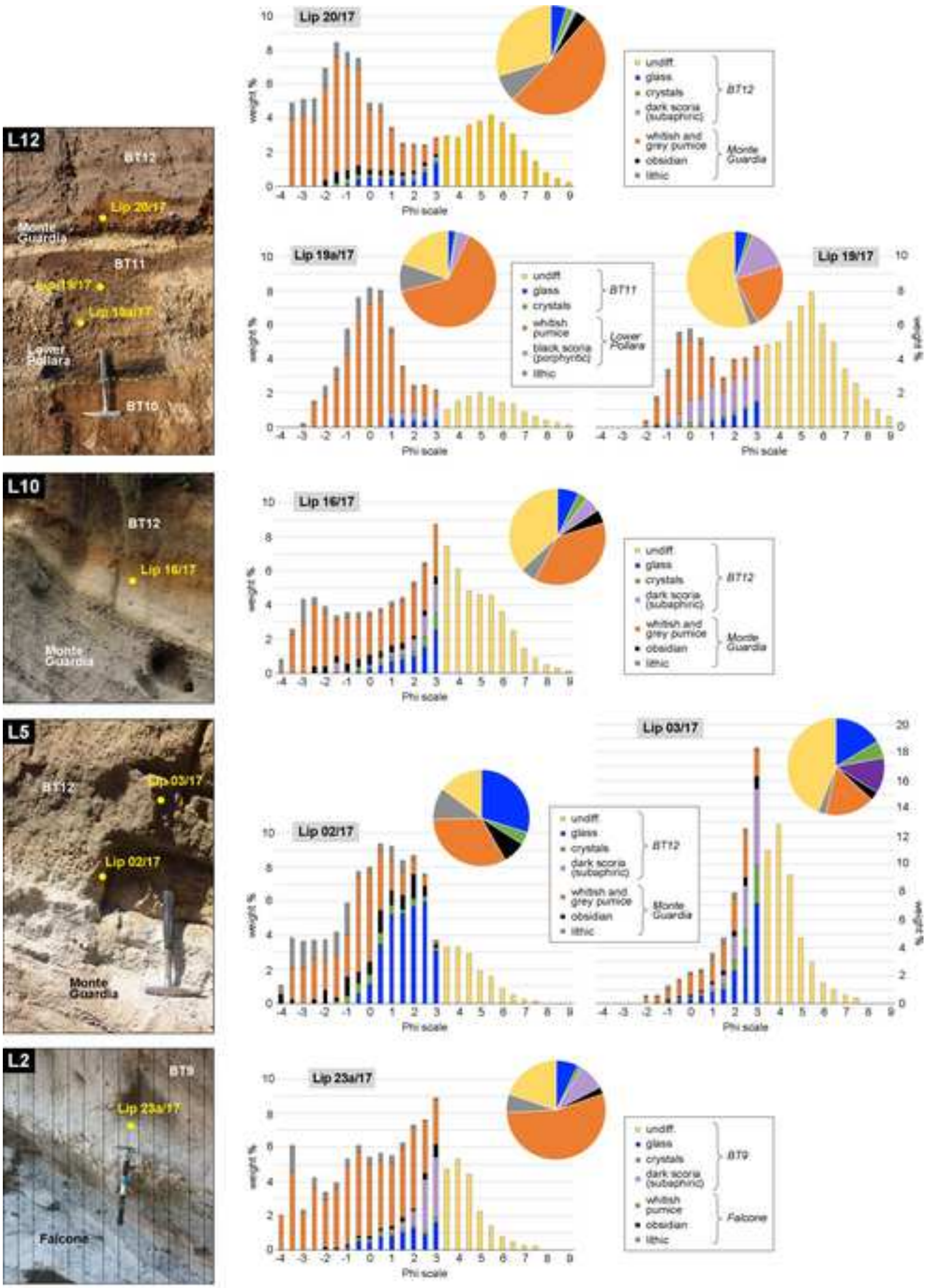
L12
BT12
Lip 20/17
Monte Guardia
BT11
Lip 19/17
Lip 19a/17
Lower Pollara
BT10
L10
BT12
Lip 16/17
Monte Guardia
L5
BT12
Lip 03/17
Lip 02/17
Monte Guardia
L2
BT9
Lip 23a/17
Falcone
Lip 20/17
undiff.
glass
crystals
dark scoria (subaphiric)
BT12
whitish and grey pumice
obsidian
lithic
Monte Guardia
Lip 19a/17
Lip 19/17
undiff.
glass
crystals
BT11
whitish pumice
black scoria (porphyritic)
lithic
Lower Pollara
Lip 16/17
Lip 02/17
Lip 03/17
Lip 23a/17
whitish pumice
obsidian
BT9
Falcone
weight %
Phi scale

Fig. 6

Figure 7 Click here to access/download;Figure;fig. 7_lucchi.jpg

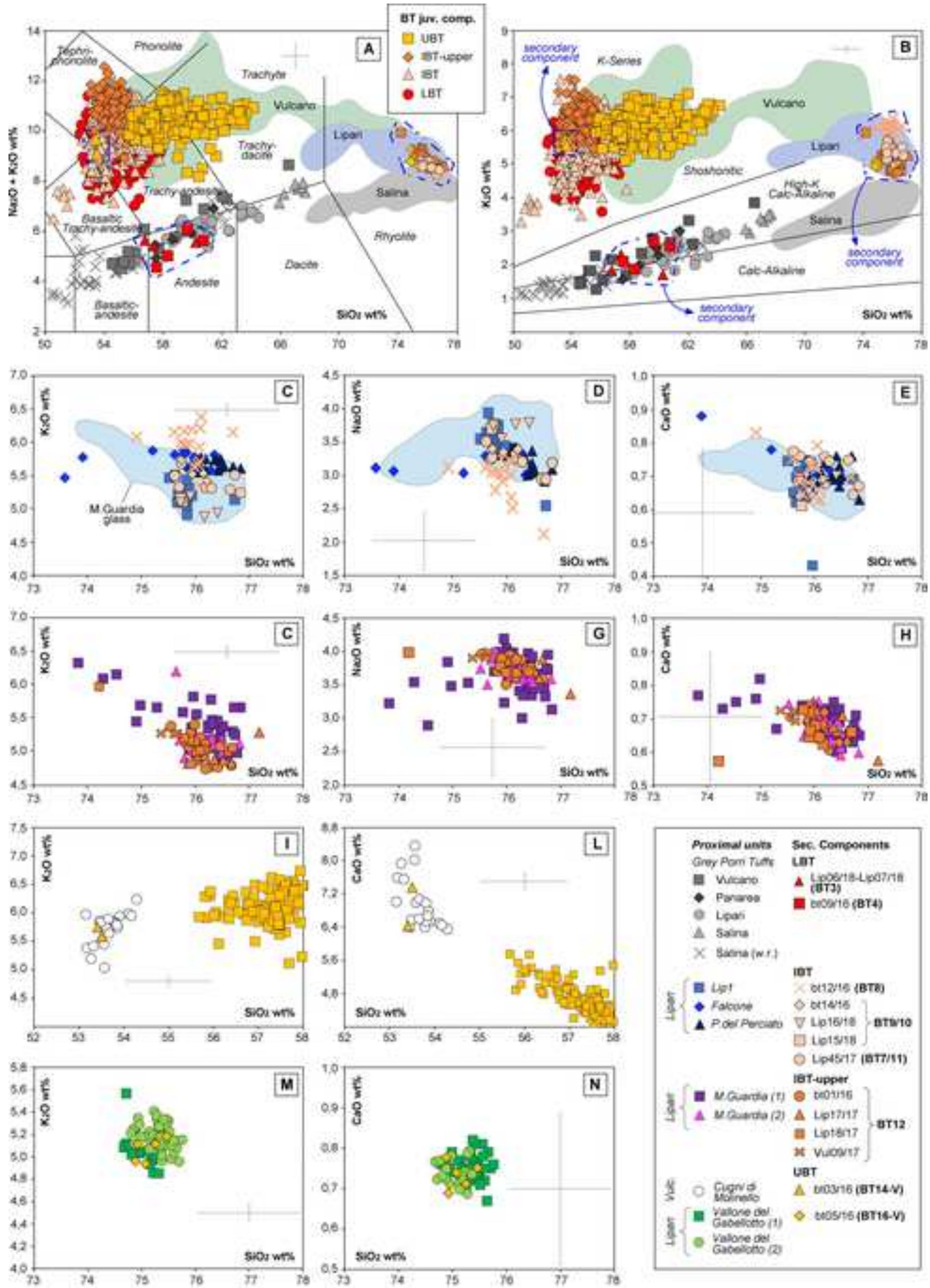

Fig. 7

Figure 8

Click here to access/download;Figure;fig. 8_lucchi.jpg

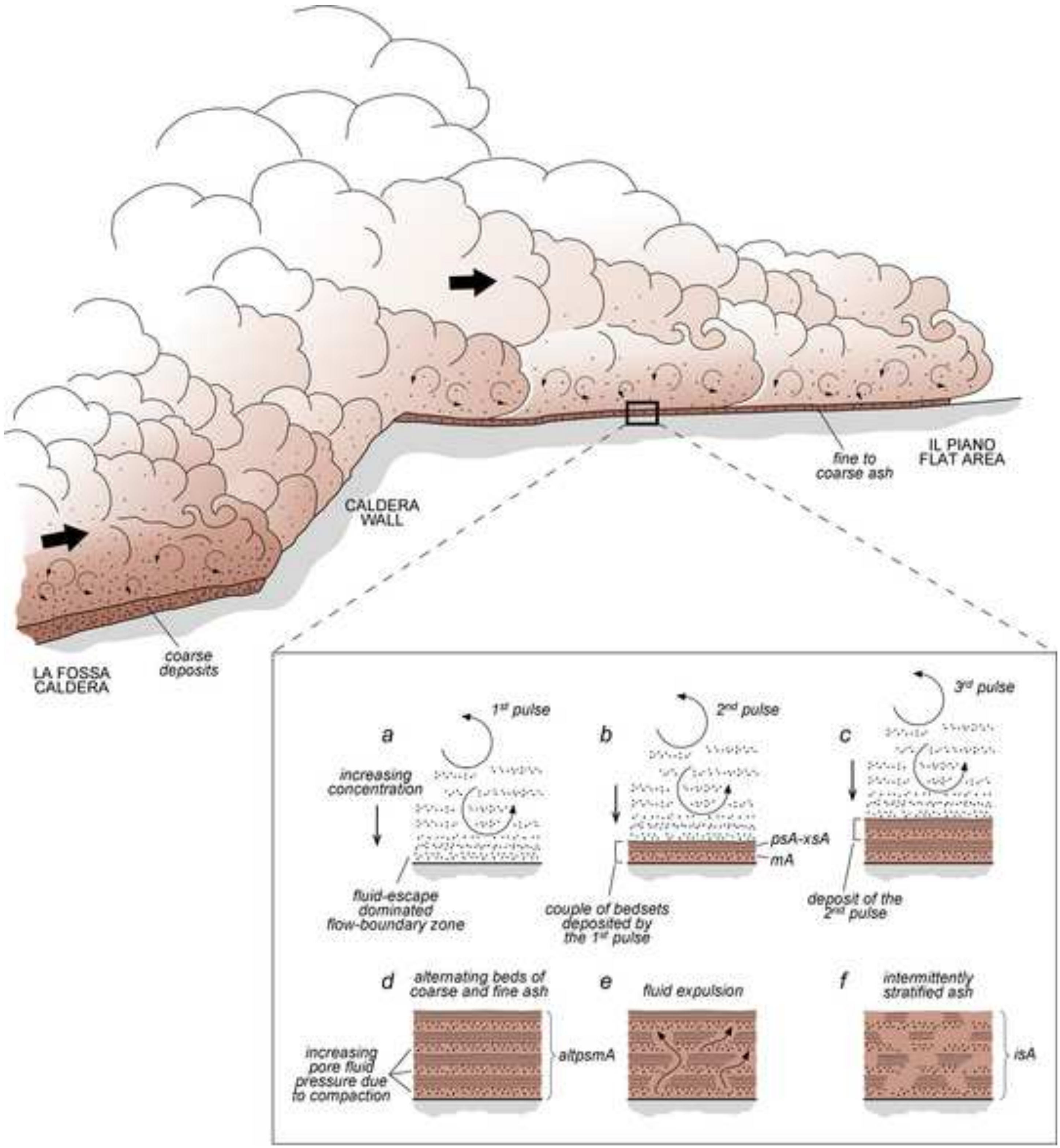

Fig. 8

Figure 9

Click here to access/download;Figure;fig. 9_lucchi.jpg

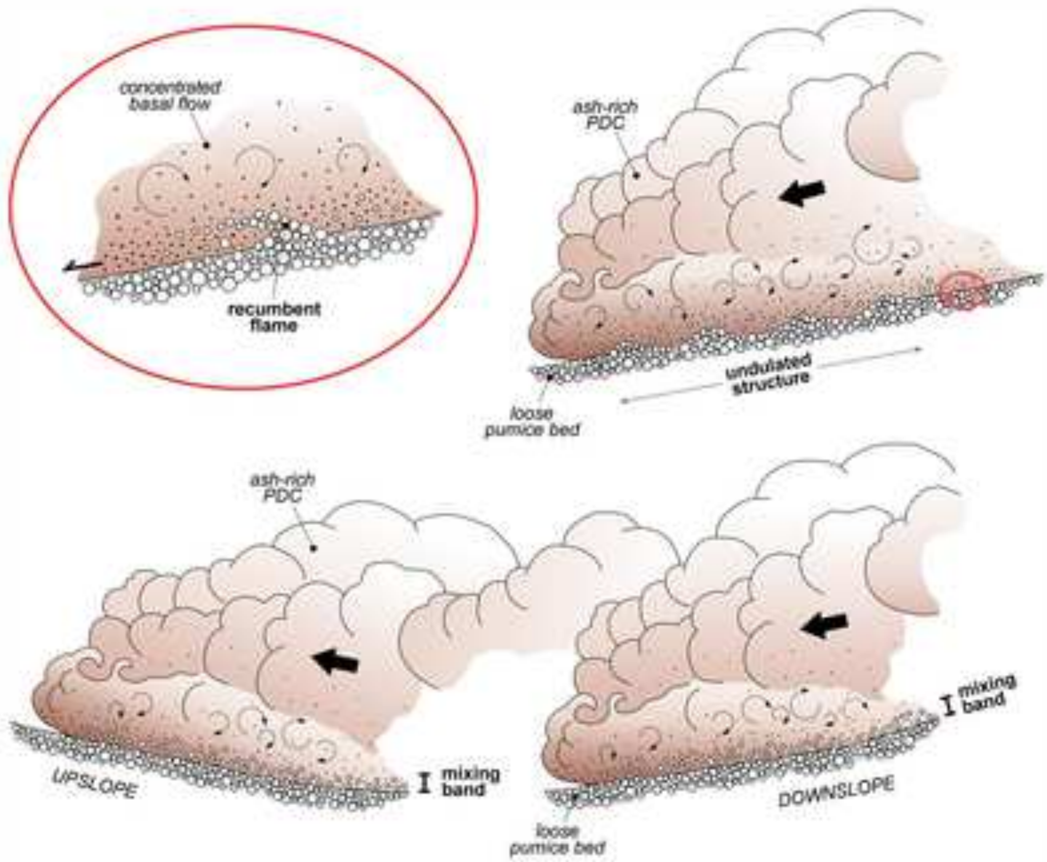

Fig. 9

Figure 10

Click here to access/download;Figure;fig. 10_lucchi.jpg

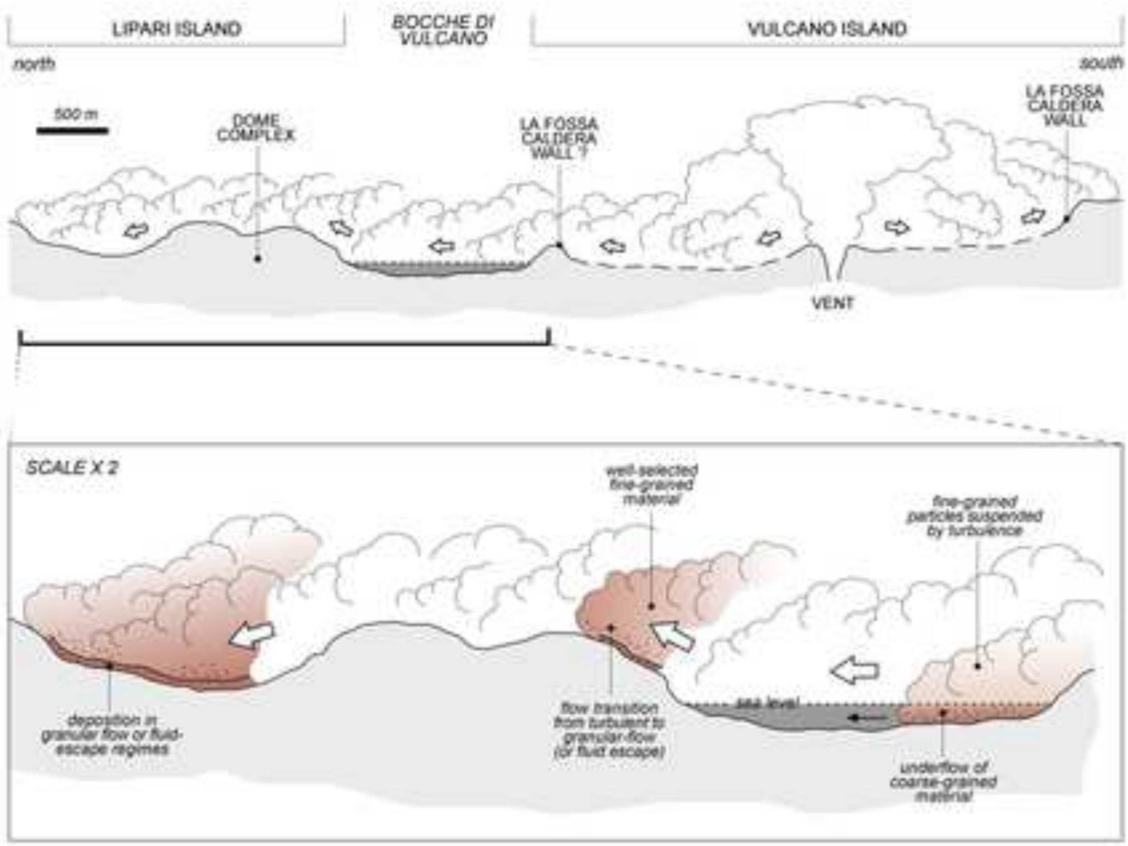

Fig. 10

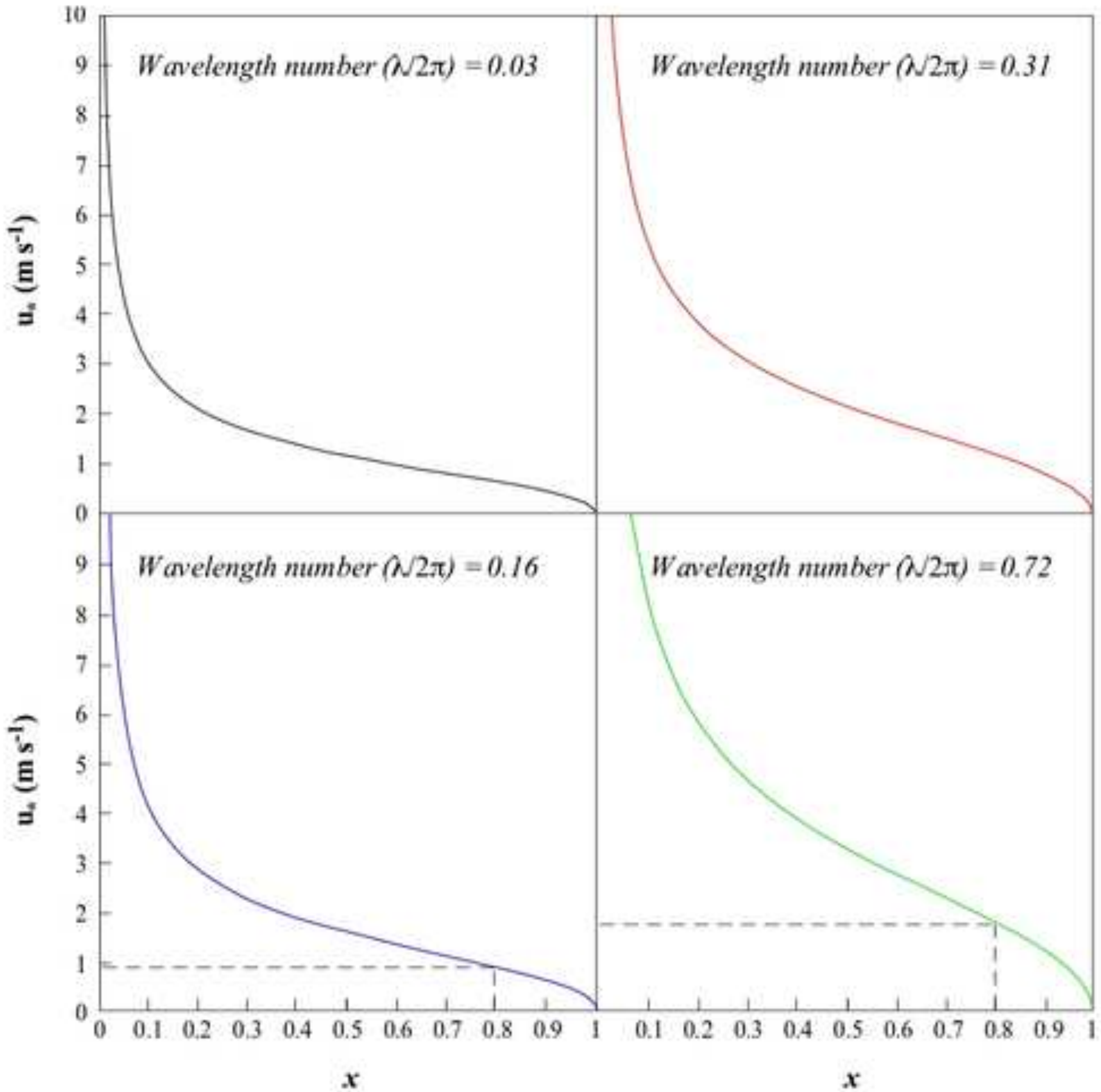
Wavelength number (λ/2π) = 0.03
Wavelength number (λ/2π) = 0.31
Wavelength number (λ/2π) = 0.16
Wavelength number (λ/2π) = 0.72
u* (m s-1)
u* (m s-1)
x
x
0
1
2
3
4
5
6
7
8
9
10
0
0.1
0.2
0.3
0.4
0.5
0.6
0.7
0.8
0.9
1

Fig. 11

Table 1 - Selected outcrops, stratigraphy and measurements of the syn-depositional sedimentary structures. The distance from the source area is arbitrarily measured relative to the centre of the La Fossa Caldera. The sample names refer to the BT depositional units selected for chemical analyses. Labels for the sedimentary structures: MB=mixing band; US=undulated structure; FS=recumbent flame structure; RS=rip-up structure. In the column of sedimentary structures the symbol / indicates that there is no direct evidence in the field of mixed lithofacies but the process of clast-embedding is outlined by means of geochemical analyses.

Island	Outcrop	Location	Distance (km)	Sedimentary structure	BT dep. unit	Sample name	underlying unit	Thickness - MB (cm)	Length (cm)	Height (cm)
Lipari	L0	Punta della Crapazza	5,5	/	BT10	Lip15/18, Lip16/18, Lip17/18	Lip1*	/		
	L1	Spiaggia Valle Muria	7,7	MB, US, FS, RS	BT9		Falcone	≈30 (max)	≈450 (US)	≈20 (US)
									≈60 (FS)	≈20 (FS)
				MB	BT10		Lip1	≈5		
	L2	Valle Muria	8.5	MB	BT11		Lower Pollara	10		
				/	BT10	bt14/16	Lip1	/		
				MB	BT9		Falcone	25-30		
				MB	BT8	bt12/16	P. di Perciato	≈10		
	L3	Chiesa dell'Annunciazion	9.5	MB	BT12		Monte Guardia	≈25		
	L4	Portinente	10	MB	BT12	bt01/16	Monte Guardia	n.v.		
	L5	Tunnel Canneto	10.5	MB, US	BT12		Monte Guardia	≈15	≈250	≈20
	L6	Vallone Canneto dentro	11	MB	BT11		Lower Pollara Tuffs	≈5		
				MB	BT9		Falcone	≈10		
				MB	BT7		Ischia Tephra	≈5		
				MB	BT3-BT4	Lip06/18, Lip07/18	Grey Porri Tuffs	≈5		
	L7	Monterosa	11	/	BT9-10-11	Lip45/17	Lip1, Falcone or P. del Perciato	/		
				MB	BT7		Ischia Tephra	≈3		
	L8	Vallone dei Lacci	12	MB	BT4	bt09/16	Grey Porri Tuffs	≈5		
	L9	Santa Margherita	11	MB	BT11		Lower Pollara Tuffs	≈10		
	L10	Madoro	12	MB	BT12	Lip17/17, Lip18/17	Monte Guardia	≈25		
				MB	BT11		Lower Pollara Tuffs	≈10		
				MB	BT9		Falcone	≈5		
	L11	Vallone Fiume Bianco	13.5	MB	BT16		Vallone del Gabellotto	≈15		
	L12	Chiesa Vecchia	14.5	MB	BT12		Monte Guardia	≈5		
				MB	BT11		Lower Pollara Tuffs	≈5		
	L13	Acquacalda	16.5	MB	BT16		Vallone del Gabellotto	≈20		
					BT12		Monte Guardia	≈10		
Vulcano	V1	Passo del Piano	2	MB	BT16 (V)	bt05/06	Vallone del Gabellotto	≈10		
	V2	Il Piano	2.5	MB	BT14 (V)		Cugni di Molinello	≈10		
	V3	Il Piano	3	MB	BT14 (V)		Cugni di Molinello	≈10		
	V4	Serra dei Pisani	4	MB	BT14 (V)	bt03/16	Cugni di Molinello	≈15		
	V5	Gelso	5.7	MB	BT12	Vul09/17	Monte Guardia	≈20		
	V6	Grotta dei Pisani	2	/	BT13(V)		Spiaggia Lunga	/		

Table 2 - Lithofacies codes, description and interpretation of the lithofacies recognized in the BT investigated in the present work. The first letters of the lithofacies code indicate the general appearance of the deposit (m = massive, ps = planar stratified, xs = cross-stratified, is = intermittently stratified, etc.) and the capital letters indicate the grain size (A = ash, L = lapilli).

Lithofacies code	**Description**	**Interpretation**	**Reference**
mA	Massive, fine to coarse ash, sometimes with scattered pumice and lapilli. Abundant ash aggregates. Geochemically homogeneous. Moderate to poor sorting.	Gentle settling from a slow-moving, ground-hugging ash cloud. The homogeneous massive appearance suggests deposition from a fine-grained, concentrated flow-boundary zone dominated by fluid escape or granular flow regime. Ash aggregates indicate the presence of steam in the ash cloud or fine ash aggregation driven by electrostatic force during gentle settling of ash from the phoenix cloud of the PDCs.	Figs. 3A, C-D, I
xsA	Cross-stratified ash, sometimes with laminae. Dune bedded, medium to coarse ash. Moderate to good sorting	Dune-bedding and internal cross stratification indicate grain by grain deposition from a diluted, turbulent current in which suspension and traction are the main transport mechanisms.	Fig. 3B
psA	Planar stratified ash, sometimes with laminae. Moderate to good sorting	Planar stratification indicate grain by grain deposition from a diluted, turbulent current in which suspension and traction are the main transport mechanisms	Fig. 3B
altpsmA	Alternating planar stratified and massive ash. Planar stratified ash sometimes contains laminae. Moderate to good sorting.	The alternating beds of planar stratified and massive ash testifies for stepwise aggradation of discrete pulses developed within each depositional unit. The massive beds indicate that the flow-boundary zone of each pulse was dominated by granular- or fluid-escape dominated depositional regime. Planar stratified ash beds testify for sedimentation from the waning stage of each pulse, mainly in the traction regime.	
isA	Intermittently stratified ash. Alternation of mm to cm thick massive and stratified beds. The stratified beds are disrupted with distinctive upward deformation and vertical columns of coarse ash at the disruption points. Moderate to good sorting	Massive beds indicate deposition from a fluid-escape dominated flow boundary zone, whilst the stratified beds indicate deposition from a dilute, turbulent current in which suspension and traction are the main transport mechanisms. The disruption of stratified beds is driven by fluid escape structures related to post depositional dissipation of pore pressure from the underlying massive beds.	Figs. 3C-H
Shear structures			
mixAL	Mixed ash and lapilli from different units. The ash component is generally homogeneous and forms the matrix of the deposit. The lapilli (and ash) fraction is made by white pumice and dark scoriae eroded from the loose underlying units. Distribution of pumice and scoria may be homogeneous or their abundance decreases regularly upwards within the overlying ash. Massive and generally poorly sorted, with occasional reverse grading of entrained coarse	Mixing of material from different units indicate erosion and incorporation of loose material from the underlying beds into the moving ash flows. The general poor sorting and massive appearance are suggestive of sedimentation from a current in which the rate of supply (Rs) is higher than the rate of deposition (Rd). This induces the rapid development of a highly concentrated zone above the flow boundary, dominated by fluid escape or granular flow regimes. The moving flow exerted shear stress over the loose substratum, causing entrapment of clasts into the flow body. The occasional reverse grading of entrained coarse clasts reveals dispersive pressure	Figs. 4A-H

	clasts.	processes induced by grain-grain collision in a high-concentration zone at the base of the current.	
ucAL	Undulated contact between ash and underlying lapilli and ash beds. The contact between the ash beds and the underlying units is represented by a transitional mixing band with wavelength of decimeters to meters. The upper part of the undulated mixed material shows imbrication of coarser clasts.	The undulated contact between ash and underlying lapilli and ash beds indicates shear exerted by the overriding flows to the loose underlying units, which induces remobilization of its upper part producing imbrication of coarse clasts and formation of waves with variable wavelength. These structures indicate high shear stress exerted by the ash flows to the substratum. Imbrication of coarse clasts testifies for the occurrence of traction carpet processes with remobilisation of the sheared material in a frictional regime.	Figs. 5A-C
rfAL	Recumbent flame structures of lapilli from the underlying beds within the ash units. The upper part of the underlying lapilli bed is ripped up and bended downflow to form an alignement of lapilli within the ash deposit.	Recumbent flame structures indicate high shear exerted by the overriding ash flows over the underlying lapilli beds, which produce incorporation of lapilli that are aligned downflow for a distance up to some meters.	Figs. 5D-E
ruAL	Rip up lapilli from the underlying beds into the ash units. Small hook-like structures visible at the contact between ash and lapilli beds. The main part of the contact is almost planar.	Small hook-like structures indicate moderate shear exerted from the overriding ash flow, which is not able to significantly displace the upper part of the underlying lapilli bed.	Fig. 5F

Table 3

Table 3. Grain size statistical parameters of Folk and Ward (1957) for the different sub-populations recognised in the samples from the base of some BT depositional units: BT=Brown Tuffs; mg=Monte guardia unit; lpt=Lower Pollara Tuffs; fa=Falcone unit. The parameters by Folk and Ward (1957) were calculated by means of the GRADISTAT program (Blott and Pye, 2001). The Sauter mean diameter (Sauter 1926) of the different BT sub-populations is estimated using the method of Breard et al. (2019).

Sample		LIP02/17		LIP03/17		LIP16/17		LIP20/17		LIP19/17		LIP19a/17		LIP23a/17	
		BT	mg	BT	mg	BT	mg	BT	mg	BT	lpt	BT	lpt	BT	fa
Median	($M\phi$)	1,98	-0,94	3,22	1,34	3,74	-0,76	4,70	-1,45	4,97	0,19	4,73	-0,22	3,13	-0,59
Mean	($\bar{x}$)	2,18	-1,09	3,25	1,05	3,80	-0,66	4,39	-1,29	4,84	0,40	4,62	-0,18	3,04	-0,64
Sorting	(s)	1,71	1,79	1,29	1,35	1,83	2,07	2,10	1,60	1,78	1,32	1,79	1,29	1,53	2,04
Skewness	(Sk)	0,19	-0,07	-0,08	-0,65	-0,29	0,10	-0,72	0,47	-0,63	0,26	-0,25	0,19	-0,28	-0,08
Kurtosis	(K)	0,93	0,89	4,01	2,45	3,40	1,75	3,31	2,65	4,17	2,07	2,69	2,77	3,25	1,89
Sauter number	(D_{32})	0,25		0,11		0,08		0,04		0,03		0,04		0,11	